Review

For reprint orders, please contact: reprints@futuremedicine.com

Nanomedicine

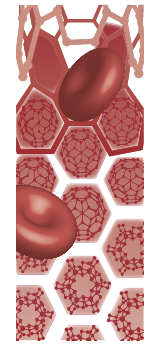

Current trends in pyrrole and porphyrin-derived nanoscale materials for biomedical applications

Parinaz Fathi[1,2] & Dipanjan Pan*[,1,2,3,4]

[1]Departments of Bioengineering, Materials Science & Engineering & Beckman Institute, University of Illinois, Urbana, IL 61801, USA

[2]Mills Breast Cancer Institute, Carle Foundation Hospital, Urbana, IL 61801, USA

[3]Departments of Diagnostic Radiology & Nuclear Medicine & Pediatrics, University of Maryland Baltimore, Health Sciences Facility III, 670 W Baltimore St., Baltimore, MD 21201, USA

[4]Department of Chemical, Biochemical & Environmental Engineering, University of Maryland Baltimore County, Interdisciplinary Health Sciences Facility, 1000 Hilltop Circle Baltimore, MD 21250, USA

*Author for correspondence: dipanjan@som.umaryland.edu

This article is written to provide an up-to-date review of pyrrole-based biomedical materials. Porphyrins and other tetrapyrrolic molecules possess unique magnetic, optical and other photophysical properties that make them useful for bioimaging and therapy. This review touches briefly on some of the synthetic strategies to obtain porphyrin- and tetrapyrrole-based nanoparticles, as well as the variety of applications in which crosslinked, self-assembled, porphyrin-coated and other nanoparticles are utilized. We explore examples of these nanoparticles' applications in photothermal therapy, drug delivery, photodynamic therapy, stimuli response, fluorescence imaging, photoacoustic imaging, magnetic resonance imaging, computed tomography and positron emission tomography. We anticipate that this review will provide a comprehensive summary of pyrrole-derived nanoparticles and provide a guideline for their further development.

Lay abstract: Nanoparticles are very small particles that are less than a fraction of the thickness of a strand of hair. These particles can be used as contrast agents (e.g., for use in a computerized axial tomography [CAT] scan) or to help deliver treatment directly to a tumor. This is a review article that explores the biomedical applications of nanoparticles formed from chemicals known as tetrapyrroles, that are often found in nature. Tetrapyrroles have many characteristics that allow them to provide good image contrast and therapeutic benefits. In this review, we discuss some characteristics of tetrapyrroles and examples of tetrapyrrole nanoparticles in a variety of biomedical applications.

First draft submitted: 25 March 2020; Accepted for publication: 14 August 2020; Published online: 25 September 2020

Keywords: bioimaging • carbon dots • drug delivery • nanoparticles • porphyrin • porphysomes • tetrapyrroles • theranostic

Porphyrin- and pyrrole-derived nanoparticles have a wide variety of applications in biomedical imaging and therapy. In this review, we begin by discussing the field of 'nano theranostics', after which we briefly describe the major imaging modalities and nanotherapeutic strategies. We then discuss the properties of porphyrins and pyrroles that make them attractive for imaging and therapeutic applications. This includes discussion of their near-infrared absorbance and fluorescence behaviors, photosensitizing behavior and ability to chelate metals. We continue by describing various examples of porphyrin- and pyrrole-derived nanoparticles, which we have categorized based on synthesis method. The bulk of this review focuses on self-assembled nanoparticles, which we have divided into categories including particles assembled from naturally-derived molecules, silica-pyrrole hybrid nanoparticles, porphysomes, dendrimers and other particles obtained through crosslinking and self-assembly. We next review examples of carbon dots or carbon nanoparticles, that have been derived from porphyrin and pyrrole molecules. Finally, we review examples in which porphyrin or pyrrole molecules were used as a coating on the surface of other

Future Medicine

nanoparticles. We conclude by discussing limitations of current approaches and provide a perspective on the future direction of research in this field.

Nanotheranostics

Small molecule heterocycles have been extensively utilized for imaging and therapeutic applications for many years [1–4]. The use of contrast agents such as methylene blue and indocyanine green is well documented [5–12]. The inspiration for using nitrogen-containing heterocycles came perhaps directly from the red color of heme, a porphyrin present in blood. Blood has served as a biomarker for assessing injury since ancient times, establishing an important role for porphyrins in the diagnosis of human diseases. The last decade has also witnessed the advent of advanced imaging techniques, such as functional MRI (fMRI) for interpretation of neural activity based on blood oxygenation [13]. The iron-containing heme can switch from diamagnetic oxyhemoglobin to paramagnetic deoxyhemoglobin allowing for the use of these properties to probe *in vivo* activities. Interestingly, porphyrins and related compounds also offer inherent optical activity that can be chemically tuned for wide ranges of light-based imaging techniques. Despite this, systemic administration of small molecule contrast agents and drugs suffers from shortcomings such as unintended off-target side effects, toxicity issues and inherent solubility issues, making these agents poorly bioavailable for target tissues.

Nanoparticles have shown great promise for diagnostic imaging and disease therapy [14–19]. Major advantages of nanoparticle-based approaches have included the ability to functionalize their surfaces for selective uptake in organs or tissues of interest [20–30], ability to load therapeutic cargo within nanoparticles [31–34] and the potential for stimuli-responsive therapeutic effects [35–42]. This has allowed for targeted imaging of diseases such as cancer and atherosclerosis, loading and release of water-insoluble drugs [43], tumor microenvironment triggered drug delivery and selective ablation of lesions. In particular, nanoparticles that provide simultaneous therapeutic and diagnostic ('theranostic') capabilities are of great interest for their multifunctionality and promise in identifying the need for therapeutic interventions and tracking their efficacy post-deployment [44,45]. An overview of theranostic applications of pyrrole-derived nanoparticles is provided in Figure 1.

Imaging modalities

A number of imaging modalities have been utilized for diagnostic imaging of diseases. Commonly used clinical imaging modalities include x-ray imaging and computed tomography (CT), ultrasound imaging, magnetic resonance imaging, positron emission tomography (PET) and single photon emission computed tomography (SPECT). An in-depth exploration of each imaging modality is beyond the scope of this review, but we will provide a brief overview of their operating principles. X-ray imaging utilizes electromagnetic radiation of frequencies ranging from 10^{16} to 10^{19} Hz. Samples of interest are exposed to x-rays, which can travel through the entire thickness of the body. A detector on the other side of the sample collects the x-rays which have passed through the sample. The density of tissues affects the ability of the radiation to pass through the sample, with samples that are denser leading to greater attenuation of the x-rays. In CT imaging, x-rays are collected for individual slices of a sample and then combined to form a 3D tomographic image. CT and x-ray imaging are commonly used for detection of cancer, bone damage, abnormalities in organs such as the heart and lungs and a variety of other applications [17,54–59].

In ultrasound imaging, a probe that generates sound in the range of 20 kHz to 200 MHz is applied to the sample. The sound waves are reflected by tissues within the body and are detected using the probe. The time taken for the sound waves to return to the probe corresponds to the distance between the probe and the tissue, allowing for the formation of an image.

MRI utilizes a strong magnetic field to align protons within the body. When the alignment of the protons is briefly disturbed using radio waves, the subsequent realignment of the protons leads to the generation of radio waves that can be detected and used in image formation. Unlike x-ray based imaging, MRI contrast agents are considered 'indirect' since they do not appear visible by themselves [60,61]. MRI contrast agents work by shortening the T1 relaxation time of protons within tissues via interactions with the neighboring contrast agent. On the contrary, x-ray contrast is generated based on their ability to absorb external x-rays, resulting in decreased exposure on the x-ray detector. Paramagnetic and superparamagnetic metal ions are used to generate high resolution (<10 μm) images of tissues, as well as to probe cellular processes at a molecular level. Typically, the efficiency of the contrast metals relies on longitudinal (r1) and transverse (r2) relaxivity. Paramagnetic metals shorten the longitudinal relaxation time (T1) and thereby increase the relaxation rate (1/T1) of solvent water protons. Regions of paramagnetic contrast agent accumulation appear bright in T1-weighted (T1w) MRI sequences and dark in T2-weighted MRI sequences.

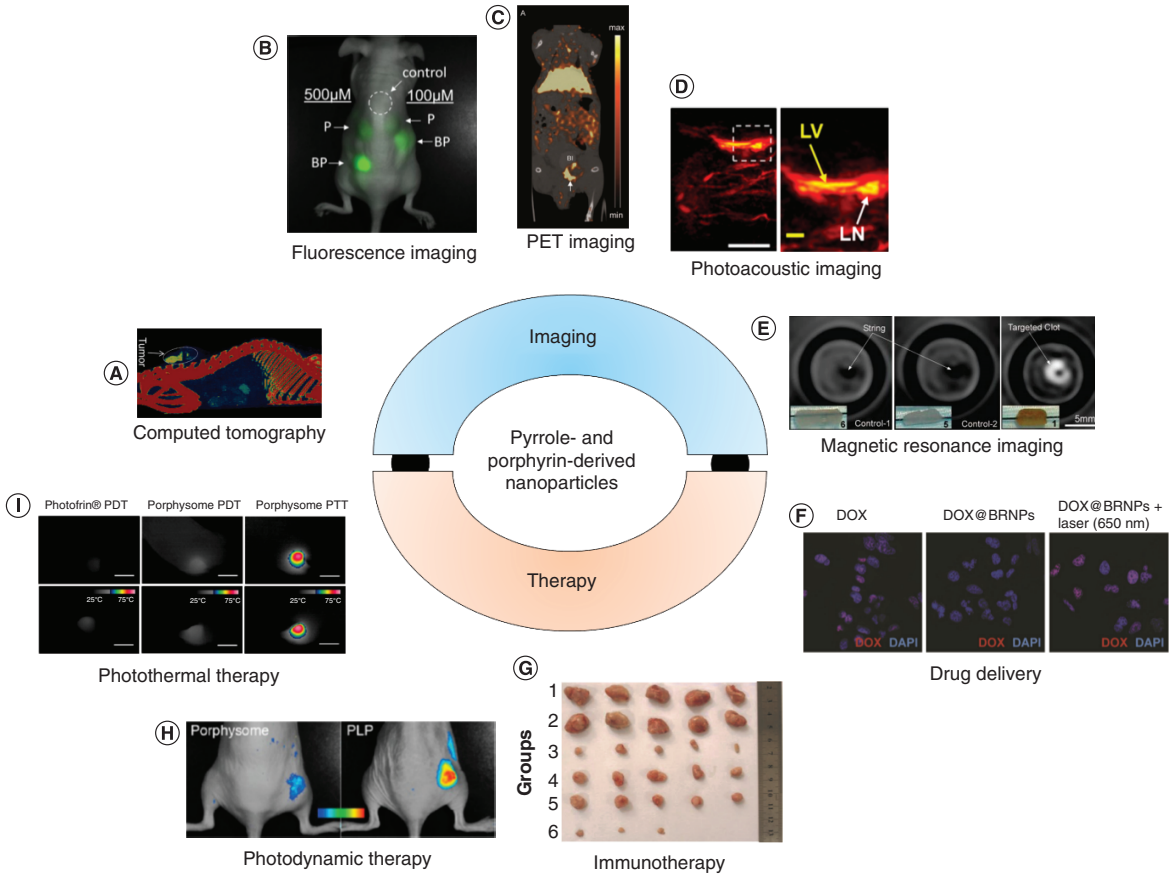

Figure 1. Applications of pyrrole- and porphyrin-derived nanoparticles. (A) Computed tomographic image of folic acid-conjugated iodinated silica-porphyrin hybrid nanoparticles accumulated in a multiple myeloma tumor. **(B)** Fluorescense image of Matrigel embedded with porphysome and Bchl-lipid doped porphysome, injected into a mouse. **(C)** PET imaging of a prostrate cancer tumor-bearing mouse 24 h after injection with ^{64}Cu-porphysomes. **(D)** Photoacoustic imaging of lymphatic vessel and lymph node of a mouse 10 min after injection of biliverdin nanoparticles (LV, LN). **(E)** MRI of blood clots using fibrin-targeted manganese-chelated nanobialys particles for contrast. **(F)** Confocal fluorescence images of A549 cells treated with DOX-loaded BRNP with and without laser irradiation. **(G)** Breast cancer tumors from mice treated with Janus nanobullets integrating chlorine e6 (Ce6) loaded, disulfide-bridged mesoporous organosilica bodies with magnetic heads. Magnetothermal therapy (group 3) and combined magnetothermal therapy/immunotherapy (group 6) led to a decrease in tumor size. **(H)** Fluorescence imaging of activation of porphysomes vs porphyliproprotein (PLP) particles 24 h after intravenous injection in KB-xenograft mice. **(I)** Temperature of tumors in mice treated with porphysomes and PDT or PTT, illustrating that photothermal therapy (right) leads to high temperatures in tumors.
BRNP: Bilirubin nanoparticle; DOX: Doxorubicin; LN: Lymph node; LV: Lymphatic vessel; PDT: Photodynamic therapy; PET: Positron emmision tomography; PLP: Porphyliproprotein; PTT: Photothermal therapy.
(A) Reproduced with permission from [46], licensed with CC-BY-NC-ND 3.0.
(B) Reproduced with permission from [47], © American Chemical Society (2015).
(C) Reproduced with permission from [48], © WILEY-VCH Verlag GmbH & Co. (2012).
(D) Reproduced with permission from [49], © American Chemical Society (2019).
(E) Reproduced with permission from [50], © American Chemical Society (2008).
(F) Reproduced with permission from [51], © WILEY-VCH Verlag GmbH & Co. (2016).
(G) Reproduced with permission from [29,46–53], licensed with CC-BY 4.0.
(H) Reproduced with permission from [52], © American Chemical Society (2015).
(I) Reproduced with permission from [53], © American Chemical Society (2013).

Iron oxide nanoparticles have been widely utilized as T2-weighted contrast agents in MRI and have been translated to clinical use for treatment of iron deficiency [62–65]. Similarly, Gd-, Mn- and copper-based agents have been used as paramagnetic contrast agents. Manganese ions (Mn^{2+}) work similarly as other paramagnetic ions, in other words, gadolinium (Gd^{3+}) and copper (Cu^{+2}), which can shorten the T1 of water protons, thus increasing the signal intensity of T1w MR images.

PET imaging makes use of radioactive nuclides to provide image contrast. As the radionuclides degrade, positrons are emitted, eventually making contact with electrons in the native tissue. The annihilation event caused by collision of the positrons and electrons leads to the generation of γ-rays in two opposite directions. The γ-rays are then simultaneously detected by two different detectors spaced 180 degrees apart, leading to the recording of an incident event. This information is then reconstructed into images. SPECT imaging detects γ-rays emitted directly from an injected radionuclide. X-rays and γ-rays are both considered ionizing radiation, which means that they can generate free radicals that lead to tissue damage. Since exposure to ionizing radiation can lead to cell death [66–68], the use of these imaging techniques must be carefully considered.

Emerging preclinical imaging techniques include fluorescence imaging and photoacoustic imaging [16,19,49,69–75]. Fluorescence imaging utilizes light of particular wavelengths to excite a fluorophore or fluorescent molecule. The absorbed light leads to excitation of the fluorophore's electrons from their ground state to a higher energy level. In downshifting, which porphyrins and tetrapyrroles are commonly used for, the subsequent return of the electrons to their ground state leads to the emission of lower-energy (higher wavelength) light. In upconversion, the absorption of multiple photons of a higher wavelength leads to the emission of light at a shorter wavelength (higher energy) than the excitation wavelength. A major drawback of fluorescence imaging is *in vivo* autofluorescence from hemoglobin in blood, which absorb light at wavelengths below 600 [76]. Thus, fluorescence imaging is often conducted in the first near-infrared (NIR-I) wavelength range of 650–950 nm. More recently, fluorescence imaging in the second near-infrared (NIR-II) range of 1000–1350 nm has grown in popularity due to reduced interference from biological tissue within this wavelength range [57,77,78].

Like fluorescence imaging, photoacoustic imaging utilizes interrogation with light to excite a light-absorbing molecule. However, in photoacoustic imaging the energy is not released through light emission upon return of excited electrons to their ground state. Instead, the absorbance of light leads to slight increases in temperature which cause thermal expansion of the material. This thermal expansion leads to the generation of sound waves which can be detected with ultrasound imaging to generate a tomographic image. Photoacoustic imaging has gained interest due to its higher spatial resolution and depth of penetration compared with fluorescence imaging. Despite this, photoacoustic imaging is still limited to a penetration depth of approximately 6 cm [79–81]. Photoacoustic responses generated from biologically available molecules such as hemoglobin and melanin lead to some interference in the NIR-I region [82–89]. Thus, photoacoustic imaging in the NIR-II region has also grown in popularity [90–92].

Nanotherapeutics

In addition to surgical interventions, a major approach in disease therapy is the administration of drugs that can lead to diseased cell death, the use of laser irradiation or magnetic fields to induce cell death, or the generation of an immune response to diseased cells through the administration of immunotherapeutic agents. Nanoparticle agents can be utilized for the encapsulation and eventual release of drugs. Nanoparticle-based drug delivery allows for the delivery of drugs with poor solubility, as well as gradual, stimuli-responsive or on-demand release of drugs and enhanced delivery of drugs to the site of interest through passive or active targeting mechanisms. In photothermal therapy [93–96], laser irradiation is utilized to irradiate a site containing nanoparticles that absorb light of the specified laser wavelength. The nanoparticles dissipate the energy from the laser through releasing heat, thus thermally ablating the surrounding tissue. In photodynamic therapy [97,98], a similar approach is taken, but the use of photosensitizers leads to the production of reactive oxygen species (ROS) in response to the laser irradiation, leading to cell and tissue death due to the ROS. Another therapeutic approach is the use of magnetothermal therapy [99–101], which utilizes alternating magnetic fields to induce heating within the tissue. In immunotherapy [102–104], administered nanoparticles can present antigens, sometimes in combination with an adjuvant, in order to activate an immune response against the diseased cells to be eradicated. Other work has focused on photoimmunotherapy for selective removal of regulatory immune cells, which leads to a subsequent increase in immune response to tumor cells [105].

Porphyrin & pyrrole characteristics

Pyrroles are organic compounds composed of a five-membered ring containing four carbons and a nitrogen. Porphyrins are composed of four modified pyrrole subunits interconnected at their α carbon atoms via methine bridges (=CH−). Other noncyclic tetrapyrrole molecules also exist. Pyrrole-derived molecules (Figure 2) have drawn interest due to their high absorbance and strong fluorescence or photoacoustic contrast, as well as their abilities to act as photosensitizers and metal chelators [55,57,64,66,84,106–111].

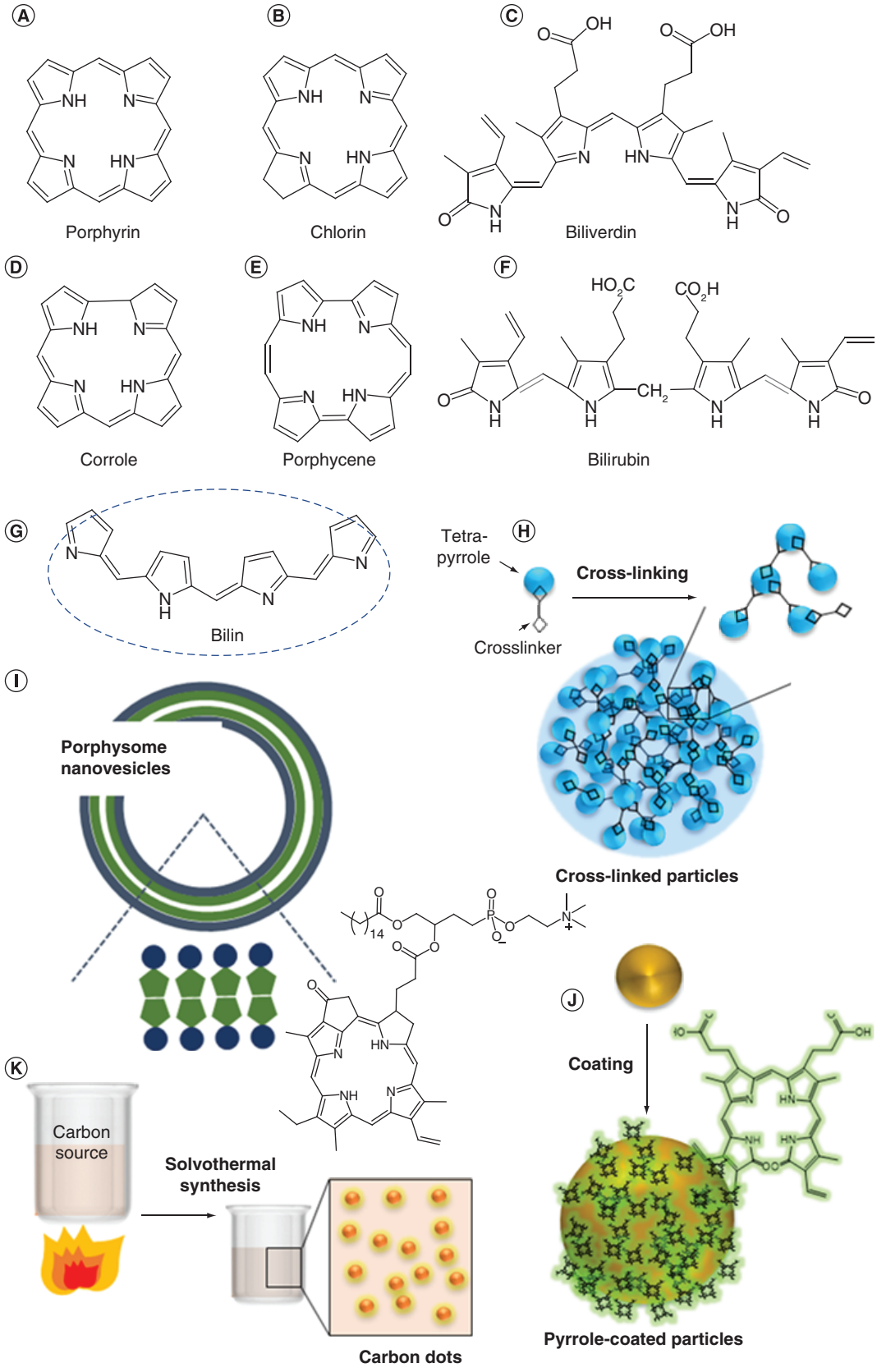

Figure 2. Open chain and macrocylic N-containing pyrrole, porphyrin and polypyrrole molecules and nanoparticles. **(A–G)** Small molecule structures; **(H)** examples of crosslinked nanoparticles from tetrapyrrole; **(I)** porphyrin conjugated lipid derived vesicles; **(J)** nanoparticles-derived from physical pyrrole coating; **(K)** carbon dots derived from porphyrin or pyrrole-based agents.

Fluorescence & absorbance properties

UV-visible absorbance spectra of porphyrin molecules typically contain a Soret band (400–436 nm), Q bands (490–650 nm) and N, L and M bands (200–350 nm) [112,113]. The Soret band, which has greater intensity than the Q bands, is attributed to the strong transition from S_0 to the second excited state S_2, whereas the Q bands are attributed to the weak transition from S_0 to the first excited state S_1 [112,113]. In addition, fluorescence yields for metal-chelated porphyrins have been shown to depend on the central metal and the radiative efficiency has been shown to depend on the presence or absence of metals [108].

Photosensitizing behavior

The photosensitizing behavior of tetrapyrroles and porphyrins has long been the topic of much research. Initial studies primarily focused on utilizing hematoporphyrin-derived photosensitizers, but other photosensitizers have been explored more recently [97,109,114,115]. The mechanism behind the photosensitizing behavior of porphyrins is explained by the excitation of a singlet photosensitizer electron caused by light, leading to excitation of a single electron into a higher-energy orbital. Through intersystem crossing, the excited singlet photosensitizer can then form an excited triplet state with a longer lifetime than the singlet state. Collision with oxygen then results in the formation of ROS and a return of the photosensitizer to its ground state [97].

Metal chelation

Porphyrins and tetrapyrroles have the potential to form coordination complexes with a variety of metals. Bivalent manganese can be chelated by porphyrins, for example, sulfonatoporphyrins, undergoing rapid oxidation to Mn (III) [111]. Manganese (III)-chelated porphyrins such as tetra-(4-sulfonatophenyl) porphyrin (TPPS4) and variations with fewer sulfonate functionalities (TPPS3, TPPS2) have also been reported [116,117]. Other porphyrin-metal complexes include uroporphyrin (UROP-1), mesoporphyrin, hematoporphyrin and metalloporphyrin (ATN-10) [118–122]. Following injection in tumor-bearing (SCC-VII) mice, paramagnetic porphyrin-Mn has been shown to provide T2-weighted MRI contrast [120]. The use of HOP-8 P (α-Aqua-13,17-bis(1-carboxypropionyl)carbamoylethyl-3,8 bis(1phenethyloxyethyl)-β-hydroxy-2,7,12,18-tetramethylporphyrinato manganese [III]) as a tumor-specific manganese-based agent has been demonstrated in a tumor-bearing mouse model [123]. Such metalloporphyrins also exist naturally. Chlorophyll, the plant pigment used in photosynthesis, is a magnesium-chelated porphyrin. Heme, the oxygen-binding domain of hemoglobin, is composed on an iron-chelated porphyrin. Metal coordination complexes have also been reported with other tetrapyrroles [124–126].

Porphyrins & pyrroles as functional building blocks

Nanoparticles derived from porphyrins and other pyrrolic compounds have been utilized in a variety of applications including fluorescence imaging, photoacoustic imaging, MRI, CT, PET, photothermal therapy, drug delivery and biosensing. Other reviews have focused on metalloporphyrin nanoparticles [105], porphyrin-loaded nanoparticles for cancer therapy [127], polypyrrole nanoparticles for photothermal therapy [128], nanoparticles derived from organic dyes [129] and porphysomes [130–132]. In this review, we have classified porphyrin and polypyrrole-derived nanoparticles into categories of cross-linked or self-assembled particles, carbon dots and coated particles. We will provide an overview of the different synthetic strategies for each class of particle and will provide examples of the wide variety of applications each class of nanoparticle has been used for.

Self-assembled particles

One synthetic strategy for polypyrrole and porphyrin nanoparticles has involved exploiting the multiplicity of their functional groups along with polymeric or short homo multifunctional crosslinkers to crosslink multiple molecules (Figure 2H) or attach ligands (Figure 2I) which would allow for self-assembly.

Naturally-derived porphyrins & pyrroles

Naturally-derived porphyrins and polypyrroles are commonly used for nanoparticles. Hemoglobin, a naturally occurring blood protein contains heme, an iron-chelated porphyrin that is utilized for oxygen transport. Heme-derived pigments have been a popular source of tetrapyrroles for self-assembled nanoparticles. One such example, bilirubin, an endogenous molecule with poor water solubility, has been extensively utilized by Jon *et al.* as a precursor for nanoparticle synthesis. In their preliminary work, Lee *et al.* took advantage of bilirubin's dual

carboxylic acid groups to attach amine-terminated polyethylene glycol to bilirubin via carbodiimide coupling, eliminating bilirubin's insolubility in water (Supplementary Figure 1) [133]. This amphiphilic pegylated bilirubin then self-assembled into nanoparticles (BRNPs) with a hydrodynamic size of 136 ± 9 nm. Lee *et al.* examined the use of BRNPs as reactive oxygen species scavengers, demonstrating the selective uptake of these particles in inflamed colons *in vivo* in mice. In addition, they found that BRNPs prevented an increase in myeloperoxidase, a marker of irritable bowel disease severity and led to a decreased expression of proinflammatory cytokines in a colitis mouse model, compared with controls that were treated with saline. Finally, in addition to traditional *in vitro* evaluation of biocompatibility, histological analysis of lung, liver, kidney and spleen samples were conducted on BRNP-treated mice 1 week after nanoparticle administration in order to demonstrate the good biocompatibility of BRNPs.

In further work, Lee *et al.* examined the use of BRNPs for stimuli-responsive anticancer therapy [51]. They determined that BRNPs experience a switch in solubility upon exposure to ROS or UV irradiation, leading to their subsequent disassembly. They demonstrated the use of this phenomenon for triggered release of doxorubicin, a chemotherapeutic drug. Mice bearing human lung adenocarcinoma xenograft tumors were shown to have reduced tumor volumes when treated with both doxorubicin-loaded BRNPs and 650 nm irradiation, compared with mice treated with doxorubicin or doxorubicin-loaded BRNPs alone. Kim *et al.* utilized BRNPs for the prevention of hepatic ischemia reperfusion injury [134]. They reasoned that since bilirubin has been shown to reduce ischemia reperfusion injury, BRNPs would have a similar preventative effect, with the added benefit of water solubility. Biocompatibility of BRNPs was demonstrated *in vivo* in mice through histopathological analysis and measurement of alanine aminotransferase (ALT), a hepatocellular damage marker, after intravenous injection of particles. In addition, the ability of BRNPs to reduce hepatocellular ischemia reperfusion injury was examined in mice. Mice that received an intravenous injection of BRNPs prior to periods of ischemia and reperfusion were found to have lower levels of serum ALT and aspartate aminotransferase (AST) compared with mice that received injections of phosphate-buffered saline or peritoneal injections of unconjugated bilirubin. Such BRNP preconditioning was also found to lead to lower apoptosis and necrosis compared with preconditioning with unconjugated bilirubin, reduced expression of pro-inflammatory cytokines, chemokines and cell adhesion molecules from ischemia reperfusion injury and inhibition of neutrophil infiltration after ischemia reperfusion.

BRNPs were found to prolong pancreatic islet graft survival in a diabetic rat model [135]. They were also demonstrated to scavenge ROS to protect islet cells from oxidative stress and suppress cytokine release to protect islet cells from activated macrophages. The anti-inflammatory properties of BRNPs also allowed for their use as an anti-asthmatic in a mouse model of allergen-induced asthma [136]. BRNPs were found to possess immunomodulatory behavior, which reduced lung inflammation and asthma symptoms. The chelation of cisplatin into BRNPs has also been explored, forming particles with a hydrodynamic size of 192 ± 88 nm. The resulting particles were used for drug delivery, photoacoustic imaging and photothermal therapy of mice bearing HT-29 human colorectal carcinoma tumors [137].

Biliverdin is another heme-derived tetrapyrrole molecule that has been utilized for nanoparticle synthesis. Recently, Fathi *et al.* reported the crosslinking of biliverdin molecules using a bifunctional amine linker to form biliverdin nanoparticles with hydrodynamic diameters of approximately 100 nm (Supplementary Figure 2) [49]. They found that the particles had high absorbance at 365 and 680 nm and could be utilized for fluorescence imaging with UV wavelengths and photoacoustic imaging with NIR wavelengths. They utilized biliverdin nanoparticles for sentinel lymph node imaging and demonstrated the complete biodegradation of these particles in the presence of biliverdin reductase. Xing *et al.* utilized biliverdin and a metal-binding peptide, Z-Histidine-Obzl, to form self-assembled biliverdin nanoparticles that contained Mn^{2+} [138]. The resulting particles were found to have hydrodynamic sizes of 120 ± 20 nm. Cells exposed to the particles alone had no significant loss of viability, while those exposed to 730 nm UV irradiation in the presence of nanoparticles were found to have a significant decrease in viability. Xing *et al.* demonstrated the ability of these particles to be used in MRI, photoacoustic imaging and photothermal therapy of MCF-7 tumors in mice.

Hemin, a heme-derived porphyrin, has also been utilized in the formation of nanoparticles. Yang *et al.* utilized dialysis of hemin dissolved in acidified acetone to form hemin nanoparticles [139]. They experimented with different temperatures, volume ratios and incubation times, finding that higher initial concentrations of hemin led to the formation of spherical particles (hydrodynamic diameters of 218.2 ± 6.2 nm), while lower initial concentrations of hemin led to the formation of tadpole-shaped particles (hydrodynamic diameters of 299.8 ± 7.6 nm). Hemin nanoparticles were also found to have a higher solubility than pure hemin. In a separate report, Liu *et al.* reported the formation of self-assembled nanoparticles from hemin, guanine-rich DNA and histidine-rich peptides [140].

Table 1. Summary of naturally derived porphyrin and tetrapyrrole particles.

Porphyrin or tetrapyrrole	Particle type	Application	Hydrodynamic diameter (nm)	Ref.
Bilirubin (tetrapyrrole)	Self-assembled	ROS scavengers, decreased inflammation in a colitis mouse model	136 ± 9	[133]
	Self-assembled	Triggered release of doxorubicin in mice bearing human lung adenocarcinoma xenograft tumors	105	[51]
	Self-assembled	Prevention of ischemia reperfusion injury	Approximately 100	[134]
	Self-assembled	Prolong pancreatic islet graft survival in diabetic rats	90 ± 2	[135]
	Self-assembled	Reduced lung inflammation and asthma symptoms in allergen-induced asthma	Approximately 100	[136]
	Self-assembled	Cisplatin delivery, photoacoustic imaging and photothermal therapy in mouse HT-29 tumors	192 ± 88	[137]
Biliverdin (tetrapyrrole)	Self-assembled and stabilized by cross-linking	Photoacoustic sentinel lymph node imaging, fluorescence imaging, biodegradability	Approximately 100	[49].
	Self-assembled	Photothermal therapy, MRI, photoacoustic imaging, MCF-7 tumor treatment	120 ± 20	[138]
Hemin (porphyrin)	Self-assembled	Increased solubility compared with pure hemin	218.2 ± 6.2 (spherical) 299.8 ± 7.6 (tadpole-shaped)	[139]
	Self-assembled	Peroxidase-mimicking activity	-	[140]

ROS: Reactive oxygen species.

These nanoparticles utilized hemin as a cofactor to exhibit peroxidase-mimicking activity and were shown to oxidize reducing substrates. A summary of naturally derived porphyrin and tetrapyrrole particles is provided in Table 1.

Silica-containing porphyrin & tetrapyrrole hybrids

In addition to the formation of amide bonds, another mechanism of nanoparticle crosslinking has been the formation of siloxane bonds. Hayashi *et al.* utilized tetrakis (4-carboxyphenyl)porphyrin (TCPP), a porphyrin, to form silica-porphyrin hybrid nanorings [141]. They utilized the carboxylic acid groups on TCPP to form amide bonds with 3-aminopropyltriethoxysilane (APTES). They then utilized APTES and tetraethylorthosilicate (TEOS) for polycondensation of TCPP-APTES into nanorings and coated the nanoparticle surface with polyethylene glycol, obtaining a final hydrodynamic diameter of 98 ± 37 nm. When injected intravenously in mice bearing tumors from human myeloma cells, these particles were found to accumulate within the tumors, which was attributed to the enhanced permeability and retention effect.

In a separate work, Hayashi *et al.* developed iodinated silica/porphyrin hybrid nanoparticles (ISP HNPs) by sol-gel reaction of porphyrin-containing silicon alkoxide (PCSA) with (3-iodopropyl)trimethoxysilane (IPTMS) [142]. ISP HNPs had an anhydrous size of 47 ± 12 nm and were utilized for fluorescence imaging, photothermal therapy and photodynamic therapy in mice bearing human myeloma tumors. Treatment of mice with ISP HNPs and light-emitting diode (LED) irradiation led to a lower tumor volume compared with mice that received no treatment or received only ISP HNPs or only LED irradiation. Mice treated with ISP HNPs and LED irradiation also had a 100% survival rate 10 weeks post treatment. Hayashi *et al.* also utilized ISP HNPs modified with PEG and targeted with folic acid to conduct *in vivo* fluorescence and CT imaging on multiple myeloma tumors in mice (Supplementary Figure 3) [46].

Others have also developed silica-porphyrin nanohybrid structures. Ohulchanskyy *et al.* synthesized iodobenzyl-pyro-silane, which they then coprecipitated with vinyltriethoxysilane to form porphyrin-containing organically modified silica nanoparticles [143]. The biocompatibility, photosensitizing properties and fluorescence capabilities of these particles were demonstrated using *in vitro* MTT assays in RIF-1 tumor cells. Qiu *et al.* reported the formation of chiral mesostructured porphyrin–silica hybrids [144] and Hayashi *et al.* reported the formation of silica–porphyrin hybrid nanotubes for *in vivo* macrophage tracking [145]. In addition to standard *in vitro* evaluation of nanoparticle toxicity, Hayashi *et al.* reported detailed *in vivo* toxicity studies using bloodwork conducted on mice one week after intravenous administration of nanoparticles. Alkaline phosphatase, alanine aminotransferase and aspartate aminotransferase levels in serum were used to evaluate liver function, while blood urea nitrogen levels in serum were used to evaluate nephrotoxicity. A summary of porphyrin–silica hybrid nanoparticles is provided in Table 2.

Table 2. Summary of porphyrin-silica hybrid nanoparticles.

Porphyrin building block	Crosslinker	Application	Ref.
TCPP	APTES and TEOS	NIR fluorescence imaging of human myeloma tumors in mice	[141]
	TMAPS	*In vivo* macrophage tracking	[145]
Porphyrin-containing silicon alkoxide	IPTMS	Fluorescence imaging, photothermal therapy and photodynamic therapy in mice bearing human myeloma tumors	[142]
		Targeted *in vivo* fluorescence and CT imaging on multiple myeloma tumors in mice	[46]
Iodobenzyl-pyro-silane	Vinyltriethoxysilane	*In vitro* photosensitizing and fluorescence imaging	[143]
TSPP	TMAPS and TEOS	–	[144]

APTES: 3-Aminopropyltriethoxysilane; CT: Computed tomography; IPTMS: (3-Iodopropyl)trimethoxysilane; TCPP: Tetrakis (4-carboxyphenyl)porphyrin; TEOS: Tetraethylorthosilicate; TMAPS: Trimethyl[3-(triethoxysilyl)-propyl]ammonium chloride; TSPP: Meso-tetra(4-sulfonatophenyl) porphyrin.

Porphysomes

Porphysomes are self-assembled nanovesicles formed from porphyrin bilayers and are a class of nanoparticle extensively studied by Lovell *et al.* and Zheng *et al.* Lovell *et al.* reported the synthesis of porphysomes using an acylation reaction to attach pyropheophorbide to lysophosphatidylcholine (Supplmementary Figure 4) [146]. The structures self-assembled and were extruded to form porphysomes of approximately 100 nm diameter. They also separately formed porphysomes of zinc-pyropheophorbide and bacteriochlorophyll. The porphysomes were utilized in photoacoustic sentinel lymph node imaging, as well as fluorescence imaging and photothermal therapy, which was evaluated in KB cell mouse xenografts. The enzymatic degradation of porphysomes was demonstrated and porphysomes were also found to have minimal *in vivo* toxicity. The biocompatibility of porphysomes was extensively evaluated both through blood tests and hematoxylin and eosin staining of the liver, spleen and kidneys. Liver function was assessed through quantification of alkaline phosphatase, γ-globulin transferase, blood urea nitrogen, cholesterol, albumin, alanine transferase and bile acid levels. Red blood cell and heme regulation were assessed by quantification of red blood cells, hemoglobin, corpuscular hemoglobin, red blood cell distribution width, corpuscular hemoglobin concentration and hematocrit. Further blood analysis was conducted to quantify white blood cells, monocytes, leukocytes, basophils, eosinophils and platelets. These experiments altogether demonstrated the highly favorable biocompatibility of porphysomes.

Liu *et al.* reported the use of ^{64}Cu-chelated porphysomes for PET imaging [48]. Radio-labelling was conducted after porphysome formation and particles were used for combined PET and CT imaging in an orthotopic PC3 prostate cancer model by taking advantage of leaky tumor vasculature. Liu *et al.* later reported the use of ^{64}Cu-chelated porphysomes for imaging prostate tumor bony metastases [147]. Jin *et al.* conducted comparative experiments the use of porphysomes and porphyrin monomers (Photofrin) for photodynamic and photothermal therapy of hypoxic and hyperoxic KB xenograft tumors (Supplementary Figure 5) [53]. They demonstrated that since photodynamic therapy relies on the presence of oxygen, porphysome-based photodynamic therapy was only effective under hyperoxic conditions. However, photothermal therapy was found to be effective under both hypoxic and hyperoxic conditions. MacLaughlin *et al.* also utilized porphysomes for photothermal therapy in a patient-derived pancreatic cancer xenograft model [148].

MacDonald *et al.* chelated Mn^{3+} into porphysomes to provide MRI contrast [149]. These particles were found to have high photostability and retained the potential for use in photothermal therapy. Ng *et al.* doped porphysomes with a bacteriopheophorbide–lipid to allow for energy transfer (forster resonance energy transfer) between pyropheophorbide and bacteriopheophorbide [47]. This was necessary because of the self-quenching behavior of regular porphysomes, which did not allow for fluorescence detection of intact porphysomes. Doping with bacteriopheophorbide allowed for fluorescence emission detection of bacteriopheophorbide for intact porphysomes and fluorescence emission detection of pyropheophorbide for disrupted porphysomes. This allowed fluorescence imaging to be utilized to determine whether the porphysomes were intact or disrupted *in vivo*.

Muhanna *et al.* used ^{64}Cu-chelated porphysomes for imaging of head and neck cancer in a rabbit model [150]. The use of ^{64}Cu-chelated porphysomes allowed for PET mapping of vascular and lymphatic vessels between the tumor and metastatic lymph nodes. Porphysome accumulation in the tumor and lymph nodes was also confirmed with fluorescence imaging. Jin *et al.* used ^{64}Cu-chelated porphysomes for MRI-guided focal photothermal therapy

Table 3. Summary of porphysomes.

Porphysome modification	Application	Ref.
Various porphyrin sources: pyropheophorbide, zinc-pyropheophorbide, bacteriochlorophyll	Fluorescence imaging, photoacoustic imaging, photothermal therapy of KB cell xenografts	[146]
^{64}Cu chelation	PET-CT imaging in orthotopic PC3 prostate cancer model	[48]
	PET-CT imaging of prostate cancer bone metastases	[147]
	PET-CT imaging of head and neck cancer and metastases in a rabbit model	[150]
	MRI-guided focal photothermal therapy of prostate tumors	[151]
	Fluorescence detection of tumors and metastases in rabbit endometrial cancer model	[153]
None	Photothermal therapy of hypoxic and hyperoxic KB xenograft tumors	[53]
	Photothermal therapy in a patient-derived pancreatic cancer xenograft model	[148]
Mn^{3+} chelation	MRI and photothermal therapy	[149]
Doping with bacteriopheophorbide–lipid	FRET to determine intactness of porphysomes	[47]
Utilized chlorin derivatives (including zinc chelate) as porphyrin source	Photoacoustic imaging of hamster cheek pouch tumor	[152]
Incorporation of redox-sensitive linkage and encapsulation of indoleamine 2,3dioxygenase (IDO)	Photoimmunotherapy of breast cancer	[154]

CT: Computed tomography; FRET: Forster resonance energy transfer; PET: Positron emission tomography.

of prostate tumors [151]. Porphysomes demonstrated high tumor selectivity and the temperature change induced by photothermal therapy was monitored with MR thermometry.

Ng *et al.* demonstrated the role of chlorin modification with a methoxy group, along with zinc chelation, in forming an assembled chlorin nanovesicle [152]. The chlorin-based porphysomes were utilized in photoacoustic imaging of hamster cheek pouch tumors. Philp *et al.* utilized porphysomes for detection of primary tumor, lymph node metastases and abdominal metastases in a rabbit model of endometrial cancer [153]. This method of cancer detection was found to have a sensitivity of 98.4% and specificity of 80.0%.

Liu *et al.* utilized a redox-activatable linkage to form a porphyrin-phospholipids conjugate used in the self-assembly of porphysomes for photoimmunotherapy [154]. This provided the porphysomes with sensitivity to the elevated glutathione level in tumors. The additional encapsulation of an indoleamine 2,3-dioxygenase (IDO) inhibitor allowed the porphysomes to serve a dual purpose as photosensitizers that could induce immunogenic cell death to provoke a systemic immune response. A summary of porphysomes is provided in Table 3.

Dendritic nanostructures from porphyrins

Dendrimers are repetitively branched macromolecules consisting of a core and spherical 3D morphology. They are typically derived from a single functional entity known as dendrons. Dendrimers carrying porphyrins were first reported by Jin *et al.* [155]. Porphyrin-based photosensitizers have been attached to the branches or encapsulated in the core of dendrimers, mimicking natural heme-containing proteins [156]. Dendritic porphyrins nanoprecipitate into tiny 5–20 nm sized particles. These particles have been widely used in preclinical imaging and therapeutic applications.

Other crosslinked & self-assembled systems from porphyrins

In addition to the aforementioned examples of assembling porphyrin and tetrapyrrole-based nanoparticles, other particles have been formed from a variety of crosslinking and self-assembly methods [157,158].

Pan *et al.* reported one of the first examples of MRI with porphyrin-chelated trivalent manganese which self assembles into a morphology that resembles red blood cells [50]. Toroidal 'nanobialys' polymer-lipid particles were developed and demonstrated for use as targeted MR theranostic agents. These particles, approximately 200 nm in size, were prepared by spontaneous self-assembly of amphiphilic hyperbranched polyethylenimine. The amphiphilic hyperbranched polyethylenimine was prepared by hydrophobic modification of hyperbranched polyethylenimine with palmitic acid. The amphiphilic polymer assumed an inverted micellar structure in the presence of anhydrous chloroform, leading to the formation of a kinetically stable complex from (III)-protoporphyrin chloride (Mn-PPC). These particles were targeted to fibrin clots and MRI studies demonstrated ionic r1 and r2 relaxivities of

Table 4. Summary of other porphyrin-based cross-linked and self-assembled particles.

Particle description	Application	Ref.
Toroidal 'Nanobialys' with porphyrin-chelated manganese	Targeted MRI of fibrin clots	[50]
Self-assembled Por–DPP particles	Photoacoustic imaging and photothermal therapy of HeLa tumors in mice	[159]
Self-assembled particles formed by synthesized Por and ZnPor molecules	Fluorescence imaging and *in vitro* photothermal ablation of HeLa cells	[160]
Nitric oxide-entrapped particles of zinc meso-tetra(4-pyridyl)porphyrin (ZnTPyP)	ROS generation and nitric oxide release to fight *Escherichia Coli* and *Staphylococcus Aureus* bacteria	[161]
COF-366 NPs formed from COFs containing tetra (p-amino-phenyl) porphyrin (TAPP)	Photoacoustic imaging, photodynamic therapy and photothermal therapy of 4T1 tumors.	[162]
Nanoparticles formed from solvent exchange based self-assembly of novel Zn-metalated porphyrins	Single oxygen generation	[163]
Mn-pyro-lipid porphysomes encapsulating gold nanoparticles	SERS probe for cellular imaging	[164]
Porphyrin nanodiscs formed by linking apolipoproteins to pyro-lipid	*In vitro* singlet oxygen generation, diffusion into collagen-rich environment	[165]
Gold-porphyrin hybrid nanoparticles from tetrakis(4-sulfonatophenyl)porphyrin and Au_{10}	-	[166]
Cyclic nanorings of Zn porphyrin	-	[167]

COF: Covalent organic framework; Por–DPP: Porphyrin–diketopyrrolopyrrole; ROS: Reactive oxygen species; SERS: Surface-enhanced Raman spectroscopy.

3.7 ± 1.1 $mmol^{-1}$ s^{-1} and 5.2 ± 1.1 $mmol^{-1}$ s^{-1} per Mn ion and particulate relaxivities of $612{,}307 \pm 7213$ $mmol^{-1}$ s^{-1} and $866{,}989 \pm 10{,}704$ $mmol^{-1}s^{-1}$ per particle, respectively.

Wu *et al.* developed porphyrin–diketopyrrolopyrrole (Por–DPP), an organic compound that utilizes porphyrin as a donor molecule and diketopyrrolopyrrole as the acceptor molecule [159]. The synthesized compound possessed a red-shifted and broadened absorbance spectrum and its amphiphilic structure allowed for its spontaneous self-assembly into nanoparticles that were used for imaging and photothermal therapy of cervical cancer tumors in mice. Yang *et al.* were able to achieve red-shifted and broadened absorption spectra in self-assembled nanoparticles composed of synthesized porphyrin-based molecules Por and ZnPor [160]. The nanoparticle self-assembly was facilitated by the introduction of hydrophilic polyethylene glycol chains and pentafiuorobenzene. The Por and ZnPor nanoparticles were found to have good biocompatibility in the absence of light and successfully killed HeLa cervical cancer cells when exposed to laser irradiation.

Wang *et al.* formed particles of zinc meso-tetra(4-pyridyl)porphyrin (ZnTPyP) through noncovalent self-assembly [161]. Through coordination with the zinc, they were able to entrap nitric oxide within the nanoparticles. Upon exposure to light, the nanoparticles produced ROS and released nitric oxide, leading to the death of *Escherichia coli* and *Staphylococcus aureus* bacteria. Wang *et al.* synthesized porphyrin-containing covalent organic frameworks (COF-366) from tetra (p-amino-phenyl) porphyrin (TAPP) [162]. COF-366 NPs were formed by ultrasonic dispersion of COF-366 and were utilized for photoacoustic imaging, photothermal therapy and photodynamic therapy in 4T1 breast cancer tumors.

Pan *et al.* showed that Zn-metalation and phenyl ethynyl functionalization remarkably improves the NIR absorbance of porphyrins through strong intramolecular and intermolecular π–π interactions of porphyrin macrocycles [163]. They synthesized two novel Zn-metalated porphyrins functionalized with symmetrical two phenyl ethynyl groups. Corresponding nanoparticles (60–80 nm) were obtained through a solvent-exchange based self-assembly approach. The particles displayed good biocompatibility, excellent photostability and strong $^1O_2$ generation ability.

Other emerging applications also include the use of metallo-porphyrin particles in a surface enhanced Raman spectroscopic application. Tam *et al.* synthesized gold nanoparticles embedded into Mn-pyro-lipid porphysomes and demonstrated the potential of in surface enhanced Raman spectroscopic-based tissue imaging application [164]. In addition to these, other micro-sized porphyrin-lipid complexes have been developed, including nanodisc particles derived from ApoA-1 and porphyrin-lipid (Supplementary Figure 6) [165].

Other work has involved more fundamental studies of porphyrin behaviors. Trapani *et al.* formed hybrid gold-porphyrin nanoparticles by mixing ten atom gold clusters (Au_{10}) with tetrakis(4-sulfonatophenyl)porphyrin (TPPS) J-aggregates under mildly acidic conditions [166]. Summerfield *et al.* formed cyclic nanorings of Zn porphyrin in a directed self-assembly process. They found that the number of porphyrin subunits had a direct impact on the arrangement of the nanorings [167]. A summary of these particles can be found in Table 4.

Table 5. Summary of porphyrin and tetrapyrrole-derived carbon dots.

Carbon source	Application	Ref.
Pheophytin	Photodynamic therapy and fluorescence imaging in 4T1-tumour bearing mice	[190]
Tetraphenylporphyrin (and its complexes with palladium and platinum)	Fe^{3+} ion sensing	[191]
Mono-hydroxylphenyl triphenylporphyrin and chitosan	Photodynamic therapy of hepatocarcinoma in a mouse xenograft model	[192]
5,10,15,20-tetrakis(4-aminophenyl)porphyrin and citric acid	Targeted photoacoustic imaging of breast cancer tumors, two-photon photodynamic therapy	[193]
Corn bract	Ratiometric detection of mercury ions	[194]
Polypyrrole nanoparticles	Improved conductivity compared with regular polypyrrole nanoparticles	[195]

Carbon dots

Carbon dots, or carbon nanoparticles, are a class of nanomaterial typically formed by burning a carbon-containing material at high temperatures (Figure 2K). These particles are known for their biocompatibility, fluorescence and ease of synthesis [168–170]. In recent years, a number of papers have been published on carbon dot fundamental properties [171,172], as well as applications in bioimaging [69,173–180], drug and gene delivery [181–186] and photothermal therapy [173,187–189]. Despite this, there have been few reports focusing on the use of porphyrins and polypyrroles as precursors in carbon dot synthesis.

Wen *et al.* utilized pheophytin, a chlorophyll derivative, for microwave synthesis of carbon dots [190]. These carbon dots were initially hydrophobic, had an anhydrous size of 5.5 nm and had a fluorescence emission maximum of approximately 680 nm. The nanoparticles were shown to have high biocompatibility through MTT assays conducted on 4T1 cells exposed to various concentrations of these particles. Wen *et al.* also demonstrated the use of pheophytin carbon dots for *in vivo* photodynamic therapy and fluorescence imaging in 4T1-tumour bearing mice. Wu *et al.* utilized tetraphenylporphyrin and its transition metal complexes with palladium and platinum to form carbon dots [191]. These carbon dots were found to have strong blue fluorescence that was quenched in the presence of Fe^{3+} ions and were utilized in sensing these ions with a limit of detection of 3.7 μM.

Li *et al.* formed porphyrin carbon dots (TPP CDs) from hydrothermal synthesis using mono-hydroxylphenyl triphenylporphyrin and chitosan (Supplementary Figure 7) [192]. TPP CDs had a size of 2.6 nm and were utilized in photodynamic therapy of hepatocarcinoma in a Hepatocarcinoma 22 (H22) mouse xenograft model. The favorable biocompatibility of TPP CDs was demonstrated using MTT assays conducted on HepG2 cells. Wu *et al.* formed carbon dots from 5,10,15,20-tetrakis(4-aminophenyl)porphyrin (TAPP) and citric acid [193]. These particles exhibited UV-visible and near-infrared absorption, which was utilized for photoacoustic imaging of breast cancer tumors treated with particles targeted using centuximab. The favorable biocompatibility of these particles was demonstrated with CCK-8 assays in HCC827, H23, MDA-MB-231 and HBL-100 cell lines and their utility in inducing tumor cell death was also demonstrated using two-photon photodynamic therapy.

Zhao *et al.* reported the synthesis of near-infrared carbon dots from corn bract, reasoning that the carbon dot behavior may stem from chlorophyll-derived porphyrins that were present in the precursor material [194]. The authors demonstrated that these carbon dots could be used in ratiometric detection of mercury ions. Li *et al.* utilized polypyrrole nanoparticles as the precursor for carbon dot synthesis [195]. The carbon dots exhibited smaller sizes (30–70 nm) and higher conductivity compared with the initial polypyrrole nanoparticles. A summary of porphyrin and tetrapyrrole-based carbon dots is provided in Table 5.

Porphyrin & polypyrrole coatings

In addition to utilizing porphyrins and tetrapyrroles as precursors for nanoparticle synthesis, other nanoparticles have been functionalized with porphyrin or tetrapyrrole coatings to make use of their unique properties (Figure 2J).

Wang *et al.* coated candle soot-derived carbon dots with porphyrin through electrostatic and π-stacking interactions [196]. They demonstrated that these particles could be used for labeling of *E. Coli* bacteria and 293T cells. Additionally, the particles were found to have peroxidase-like activity, which was utilized in the development of a colorimetric glucose sensor. Arcudi *et al.* coated nitrogen-doped carbon dots with porphyrin through coupling carboxylic acid groups with amine groups [197]. In a similar approach, Huang *et al.* coated carbon dots through surface passivation with an amine-terminated poly(ethyleneglycol) followed by EDC-NHS cross-coupling with chlorin e6 [198]. The coating and carbon dots interacted via forster resonance energy transfer to provide strong

Table 6. Porphyrin- and tetrapyrrole-derived nanoparticle coatings.

Particle core	Coating (method)	Application	Ref.
Carbon nanoparticles from candle soot	Porphyrin (electrostatic and π-stacking)	Colorimetric glucose sensor	[167]
Nitrogen-doped carbon nanodots	Covalent linkage	-	[197]
Carbon dots	Chlorin e6 (EDC-NHS covalent linkage)	Fluorescence image-guided PDT of MGC803 mouse gastric cancer	[198]
Mesoporous silica nanoparticles	Bilirubin (nitrogen-protected silica template method)	Brain cancer imaging (PET, photoacoustic, ultrasound) and therapy	[199]
Silver nanoparticles	Polyvinylpyrrolidone (UV-induced polymerization)	-	[200]
Gold nanoparticles on TiO_2 substrate	Polypyrrole (plasmon induced charge separation)	-	[201]
Gold nanoparticles	Alkyl-substituted pyrrole, bithiophene and terthiophene thiols, terthiophene and sexithiophene dithiols and polythiophene polythiol (self-assembly)	-	[202]

EDC: 1-Ethyl-3-(3-dimethylaminopropyl)carbodiimide; NHS: N-Hydroxysuccinimide; PDT: Photodynamic therapy; PET: Positron emission tomography.

fluorescence emission in the near-infrared region. This allowed for their application in image-guided photodynamic therapy (PDT) in an *in vivo* mouse model of gastric cancer.

Shan *et al.* developed organosilica-based hollow mesoporous bilirubin nanoparticles for the coencapsulation of graphene oxide and tirapazamine, a bioreactive prodrug [199]. The resulting particles possessed a core-shell structure, where the core consisted of a mesoporous silica nanoparticle and the shell was composed of bilirubin-silane. The particles were utilized to scavenge H_2O_2 byproducts of aerobic glycometabolism caused by graphene oxide aerobic glycometabolism. This allowed for the protection of normal tissues from oxidative damage while inducing tumor hypoxia to convert nontoxic tirapazamine into a highly toxic radical. *In vivo* application of these particles for PET imaging, ultrasound imaging, photoacoustic imaging and cancer therapy was demonstrated in a U87MG brain cancer model.

Other efforts have focused on coating metallic nanoparticles with polypyrroles. Yang *et al.* developed a core-shell structure in which the shell consisted of a polypyrrole and the core consisted of silver nanoparticles [200]. Takahashi *et al.* utilized plasmon induced charge separation to coat gold nanoparticles with polypyrrole [201], while Zotti *et al.* formed self-assembled monolayers on gold nanoparticles [202]. A summary of porphyrin- and tetrapyrrole-derived nanoparticle coatings is presented in Table 6.

Limitations

Porphyrins and pyrrole-derived nanomaterials find widespread preclinical use because of their large extinction coefficients, excellent biocompatibility and negligible adverse effects on organisms. Despite the many advantages of utilizing porphyrins and tetrapyrroles for nanomedicine, a number of drawbacks exist. First, a majority of these materials are used for fluorescence imaging, which faces inherent limitations in depth of penetration and spatial resolution. Second, the overlap of porphyrin and tetrapyrrole absorbance and fluorescence spectra with those of biological components such as blood can lead to difficulties in distinguishing between background signal and the signal from contrast agents. Third, for many metal-chelated compounds, including porphyrins and tetrapyrroles, the possibility for unintended release of metal ions must be taken into consideration.

Strong efforts are being devoted to address these issues. For example, although porphyrin derivatives have been extensively used for fluorescence imaging, PDT and photothermal therapy (PTT), the absorption maxima of many porphyrin derivatives are generally below 700 nm [203] and they typically exhibit poor photostability in NIR treatment, which limits their shelf-life and long-term use [204]. A possible way to counter these issues is to redshift the Q-band absorption to near 800 nm through enhancing their π-conjugated system. For example, introducing functionalities such as DPP that can enhance their molar absorption coefficient and photostability. DPP offers a unique electron-deficient feature and when conjugated with electron-donating components to form a donor–acceptor structure, it enhances their NIR absorption [205].

Conclusion

Porphyrin- and pyrrole-derived nanoparticles have proven promising in a variety of biomedical applications including CT imaging, fluorescence imaging, MRI, photoacoustic imaging, drug delivery, photothermal therapy, immunotherapy and photodynamic therapy. Among the favorable properties of these nanoparticles are high near-

infrared absorbance and fluorescence, chelation of metals and photosensitizing behavior. Porphyrin- and pyrrole-derived nanoparticles have been achieved through a variety of synthetic routes. Such nanoparticles have been heavily utilized in diagnosis and treatment of cancers, including endometrial cancer, breast cancer, prostate cancer, pancreatic cancer, brain cancer, gastric cancer, liver cancer and cervical cancer. Less commonly, such nanoparticles have been utilized in treatment of other conditions such as ischemia reperfusion injury or colitis, in prolonging pancreatic islet graft survival or tracking macrophages. Porphyrins and pyrroles are highly promising functional building blocks with strong potential for further use in biomedical applications.

Future perspective

Porphyrin- and tetrapyrrole-based nanoparticles are promising tools for bioimaging, therapeutic and sensing applications. These particles can be made through a variety of synthesis methods including cross-linking, self-assembly, hydrothermal synthesis and other techniques. Porphyrin- and tetrapyrrole-based nanoparticles have been demonstrated to have a variety of applications in fluorescence imaging, photoacoustic imaging, MRI, CT imaging, PET imaging, photothermal therapy, photodynamic therapy and drug delivery. In addition, these nanoparticles have been shown in some cases to exhibit biodegradability and stimuli-responsive behaviors that make them a promising platform with some inherent advantages over traditional nanoparticles.

Further studies must be conducted to better explore the use of porphyrins and tetrapyrroles in clinically-available imaging modalities while taking into consideration the potential toxicity issues that may arise from the introduction of these materials into the body. For example, the development of PEGylation-free porphyrin-based nanoparticles allows for reduced concern about immunogenicity of poly(ethylene glycol) coatings that are often used to increase nanoparticle circulation time [52]. The use of these porphyrin-high-density-lipoprotein particles has been demonstrated for lung cancer therapy [203]. The biocompatibility of porphyrin- and tetrapyrrole-derived nanoparticles has primarily been evaluated using traditional *in vitro* cell viability assays such as MTT assays and CCK-8 assays. There have been few reported intensive investigations of the long-term biocompatibility of these nanoparticles via bloodwork and histological analysis. Additional efforts must be undertaken to utilize nanoparticle synthesis methods that take advantage of biocompatible and biodegradable materials that prevent long-term accumulation and immunogenicity and to evaluate the long-term biocompatibility and biodegradability of these particles in a rigorous manner.

Executive summary

Background

- Pyrrole-derived nanoparticles have been used in a variety of imaging applications including MRI, positron emission tomography (PET)/single photon emission computed tomography, computed tomography, photoacoustic imaging and fluorescence imaging.
- Pyrrole-derived nanoparticles have been used in a wide variety of therapeutic applications, including drug delivery, photothermal therapy, immunotherapy and photodynamic therapy.

Porphyrin & pyrrole characteristics

- Porphyrin and other pyrrolic molecules possess near-infrared absorbance/fluorescence properties, which make them useful for fluorescence and photoacoustic imaging, as well as photo-based therapies.
- These molecules have photosensitizing properties.
- These molecules can chelate metals for additional contrast (e.g, chelation of manganese for MRI contrast or chelation of ^{64}Cu for PET imaging) or to improve photothermal properties (e.g., chelation of platinum for photothermal therapy).

Types of particles

- Self-assembled: examples of self-assembled particles include nanoparticles derived from heme-based molecules, silica-porphyrin hybrid particles and porphysomes.
  - Nanoparticles formed from heme-based molecules have been extensively utilized in photoacoustic imaging, photothermal therapy, drug delivery and as anti-inflammatory therapies.
  - Hybrid silica-porphyrin particles have been used for multimodal fluorescence imaging and computed tomography.
  - Porphysomes have been utilized in photodynamic therapy, photothermal therapy, MRI, PET imaging, fluorescence imaging, photoacoustic imaging and a variety of other theranostic applications.
- Carbon dots: carbon dots formed from pyrrole-based molecules are not common, but have been utilized for metal ion sensing, photodynamic therapy, fluorescence imaging and photoacoustic imaging.
- Coated particles: pyrrolic coatings have been utilized on metal, silica and carbon nanoparticles. These coatings have lended their photophysical properties for use in fluorescence imaging and photodynamic therapy.

Supplementary data

To view the supplementary data that accompany this paper please visit the journal website at: www.futuremedicine.com/doi/suppl/nnm-2020-0125

Author contributions

P Fathi and D Pan contributed to conceptualization and writing of the review article.

Financial & competing interests disclosure

This work was funded through grants from National Institute of Health (R03EB028026) and University of Illinois. This work was also supported by the National Institute of Biomedical Imaging and Bioengineering R03EB028026 of the National Institutes of Health under Award Number T32EB019944. P Fathi was supported by the National Physical Science Consortium and the National Institute of Standards & Technology through an NPSC graduate fellowship and by the Nadine Barrie Smith Memorial Fellowship from the Beckman Institute. D Pan is the founder/co-founder of three university-based start-ups. None of these entities, however, supported this work. The authors have no other relevant affiliations or financial involvement with any organization or entity with a financial interest in or financial conflict with the subject matter or materials discussed in the manuscript apart from those disclosed.

No writing assistance was utilized in the production of this manuscript.

References

Papers of special note have been highlighted as: • of interest; •• of considerable interest

1. Sinha SH, Owens EA, Feng Y *et al.* Synthesis and evaluation of carbocyanine dyes as PRMT inhibitors and imaging agents. *Eur. J. Med. Chem.* 54, 647–659 (2012).
2. Bhardwaj V, Gumber D, Abbot V, Dhiman S, Sharma P. Pyrrole: a resourceful small molecule in key medicinal hetero-aromatics. *RSC Adv.* 5(20), 15233–15266 (2015).
3. Martins P, Jesus J, Santos S *et al.* Heterocyclic anticancer compounds: recent advances and the paradigm shift towards the use of nanomedicine's tool box. *Molecules* 20(9), 16852–16891 (2015).
4. Krall N, Pretto F, Decurtins W, Bernardes GJL, Supuran CT, Neri D. A small-molecule drug conjugate for the treatment of carbonic anhydrase IX expressing tumors. *Angew. Chem. Int. Ed. Engl.* 53(16), 4231–4235 (2014).
5. Schaafsma BE, Mieog JSD, Hutteman M *et al.* The clinical use of indocyanine green as a near-infrared fluorescent contrast agent for image-guided oncologic surgery. *J. Surg. Oncol.* 104(3), 323–332 (2011).
6. Carr JA, Franke D, Caram JR *et al.* Shortwave infrared fluorescence imaging with the clinically approved near-infrared dye indocyanine green. *Proc. Natl Acad. Sci. USA* 115(17), 4465–4470 (2018).
7. Varghese P, Abdel-Rahman AT, Akberali S, Mostafa A, Gattuso JM, Carpenter R. Methylene blue dye – a safe and effective alternative for sentinel lymph node localization. *Breast J.* 14(1), 61–67 (2008).
8. Simmons R, Thevarajah S, Brennan MB, Christos P, Osborne M. Methylene blue dye as an alternative to isosulfan blue dye for sentinel lymph node localization. *Ann. Surg. Oncol.* 10(3), 242–247 (2003).
9. Ji YB, Lee KJ, Park YS, Hong SM, Paik SS, Tae K. Clinical efficacy of sentinel lymph node biopsy using methylene blue dye in clinically node-negative papillary thyroid carcinoma. *Ann. Surg. Oncol.* 19(6), 1868–1873 (2012).
10. Otto M. Looking toward basic science for potential drug discovery targets against community-associated MRSA. *Med. Res. Rev.* 30(1), 1–22 (2009).
11. Alander JT, Kaartinen I, Laakso A *et al.* A Review of indocyanine green fluorescent imaging in surgery. *Int. J. Biomed. Imaging* 2012, 940585 (2012).
12. Thevarajah S, Huston TL, Simmons RM. A comparison of the adverse reactions associated with isosulfan blue versus methylene blue dye in sentinel lymph node biopsy for breast cancer. *Am. J. Surg.* 189(2), 236–239 (2005).
13. Blamire AM, Ogawa S, Ugurbil K *et al.* Dynamic mapping of the human visual cortex by high-speed magnetic resonance imaging. *Proc. Natl Acad. Sci. USA* 89(22), 11069–11073 (1992).
14. Yang W, Zhu G, Wang S *et al. In Situ* dendritic cell vaccine for effective cancer immunotherapy. *ACS Nano* 13(3), 3083–3094 (2019).
15. Dobrucki L, Pan D, Smith A. Multiscale imaging of nanoparticle drug delivery. *Curr. Drug Targets* 16(6), 560–570 (2015).
16. Pan D, Pramanik M, Wickline SA, Wang LV, Lanza GM. Recent advances in colloidal gold nanobeacons for molecular photoacoustic imaging. *Contrast Media Mol. Imaging* 6(5), 378–388 (2011).
17. Pan D, Schirra CO, Wickline SA, Lanza GM. Multicolor computed tomographic molecular imaging with noncrystalline high-metal-density nanobeacons. *Contrast Media Mol. Imaging* 9(1), 13–25 (2014).
18. Pan D, Pham CTN, Weilbaecher KN, Tomasson MH, Wickline SA, Lanza GM. Contact-facilitated drug delivery with Sn_2 lipase labile prodrugs optimize targeted lipid nanoparticle drug delivery. *Wiley Interdiscip. Rev. Nanomed. Nanobiotechnol.* 8(1), 85–106 (2016).

19. Pan D, Kim B, Wang LV, Lanza GM. A brief account of nanoparticle contrast agents for photoacoustic imaging. *Wiley Interdiscip. Rev. Nanomed. Nanobiotechnol.* 5(6), 517–543 (2013).
20. Zhou W, Shao J, Jin Q, Wei Q, Tang J, Ji J. Zwitterionic phosphorylcholine as a better ligand for gold nanorods cell uptake and selective photothermal ablation of cancer cells. *Chem. Commun.* 46(9), 1479–1481 (2010).
21. Jose S, Cinu TA, Sebastian R *et al.* Transferrin-conjugated docetaxel–PLGA nanoparticles for tumor targeting: influence on MCF-7 cell cycle. *Polymers (Basel)* 11(11), 1905 (2019).
22. Harris JC, Scully MA, Day ES. Cancer cell membrane-coated nanoparticles for cancer management. *Cancers (Basel)* 11(12), 1–19 (2019).
23. Wu PH, Opadele AE, Onodera Y, Nam JM. Targeting integrins in cancer nanomedicine: applications in cancer diagnosis and therapy. *Cancers (Basel)* 11(11), 1–24 (2019).
24. Martín-Rapun R, De Matteis L, Ambrosone A, Garcia-Embid S, Gutierrez L, de la Fuente JM. Targeted nanoparticles for the treatment of Alzheimer's disease. *Curr. Pharm. Des.* 23(13), 1927–1952 (2017).
25. Garbuzenko OB, Kuzmov A, Taratula O, Pine SR, Minko T. Strategy to enhance lung cancer treatment by five essential elements: inhalation delivery, nanotechnology, tumor-receptor targeting, chemo- and gene therapy. *Theranostics* 9(26), 8362–8376 (2019).
26. Dupont D, Brullot W, Bloemen M, Verbiest T, Binnemans K. Selective uptake of rare earths from aqueous solutions by EDTA-functionalized magnetic and nonmagnetic nanoparticles. *ACS Appl. Mater. Interfaces* 6(7), 4980–4988 (2014).
27. Piao X, Yin H, Guo S, Wang H, Guo P. RNA nanotechnology to solubilize hydrophobic antitumor drug for targeted delivery. *Adv. Sci.* https://doi.org/10.1002/advs.201900951, 1–7 (2019) (Epub ahead of print).
28. Taschauer A, Polzer W, Alioglu F *et al.* Peptide-targeted polyplexes for aerosol-mediated gene delivery to CD49f-overexpressing tumor lesions in lung. *Mol. Ther. Nucleic Acids.* 18, 774–786 (2019).
29. Wang Z, Zhang F, Shao D *et al.* Janus nanobullets combine photodynamic therapy and magnetic hyperthermia to potentiate synergetic anti-metastatic immunotherapy. *Adv. Sci.* 6(22), 1901690 (2019).
30. Pereira I, Sousa F, Kennedy P, Sarmento B. Carcinoembryonic antigen-targeted nanoparticles potentiate the delivery of anticancer drugs to colorectal cancer cells. *Int. J. Pharm.* 549(1–2), 397–403 (2018).
31. Deng H, Dong A, Song J, Chen X. Injectable thermosensitive hydrogel systems based on functional PEG/PCL block polymer for local drug delivery. *J. Control. Rel.* 297, 60–70 (2019).
32. Liu Y, Gong CS, Dai Y *et al. In situ* polymerization on nanoscale metal-organic frameworks for enhanced physiological stability and stimulus-responsive intracellular drug delivery. *Biomaterials* 218, 119365 (2019).
33. Deng H, Lin L, Wang S *et al.* X-ray-controlled bilayer permeability of bionic nanocapsules stabilized by nucleobase pairing interactions for pulsatile drug delivery. *Adv. Mater.* 31(37), 1–8 (2019).
34. Yu G, Zhu B, Shao L *et al.* Host−guest complexation-mediated codelivery of anticancer drug and photosensitizer for cancer photochemotherapy. *Proc. Natl Acad. Sci. USA* 116(14), 6618–6623 (2019).
35. Fan W, Yung BC, Chen X. Stimuli-responsive NO release for on-demand gas-sensitized synergistic cancer therapy. *Angew. Chem. Int. Ed. Engl.* 57(28), 8383–8394 (2018).
36. Yang Z, Song J, Tang W *et al.* Stimuli-responsive nanotheranostics for real-time monitoring drug release by photoacoustic imaging. *Theranostics* 9(2), 526–536 (2019).
37. Huang P, Wang G, Su Y *et al.* Stimuli-responsive nanodrug self-assembled from amphiphilic drug-inhibitor conjugate for overcoming multidrug resistance in cancer treatment. *Theranostics* 9(20), 5755–5768 (2019).
38. Huang X, Deng G, Han Y *et al.* Right Cu_2−xS@MnS core–shell nanoparticles as a photo/H_2O_2-responsive platform for effective cancer theranostics. *Adv. Sci.* 6(20), 1901461 (2019).
39. Guo F, Li G, Ma S, Zhou H, Chen X. Multi-responsive nanocarriers based on β-CD-PNIPAM star polymer coated MSN-SS-Fc composite particles. *Polymers (Basel)* 11(10), 1716 (2019).
40. Liu Y, Gong CS, Dai Y *et al. In situ* polymerization on nanoscale metal-organic frameworks for enhanced physiological stability and stimulus-responsive intracellular drug delivery. *Biomaterials* 218, 119365 (2019).
41. Mir M, Ahmed N, Permana AD, Rodgers AM, Donnelly RF, Rehman A. Enhancement in site-specific delivery of carvacrol against methicillin resistant *Staphylococcus aureus* induced skin infections using enzyme responsive nanoparticles: a proof of concept study. *Pharmaceutics* 11(11), 606 (2019).
42. Xu C, Gao F, Wu J *et al.* Biodegradable nanotheranostics with hyperthermia-induced bubble ability for ultrasound imaging–guided chemo-photothermal therapy. *Int. J. Nanomedicine* 14, 7141–7153 (2019).
43. Datta S, Misra SK, Saha ML *et al.* Orthogonal self-assembly of an organoplatinum(II) metallacycle and cucurbit[8]uril that delivers curcumin to cancer cells. *Proc. Natl Acad. Sci. USA* 115(32), 8087–8092 (2018).
44. Pan D. Theranostic nanomedicine with functional nanoarchitecture. *Mol. Pharm.* 10(3), 781–782 (2013).
45. Pan D. Next generation gene delivery approaches: recent progress and hurdles. *Mol. Pharm.* 12(2), 299–300 (2015).

46. Hayashi K, Wataru S, Yogo T. Iodinated silica/porphyrin hybrid nanoparticles for x-ray computed tomography/fluorescence dual-modal imaging of tumors. *J. Asian Ceram. Soc.* 2(4), 429–434 (2014).

- **Illustrates the ability of an iodinated crosslinker to be utilized to crosslink porphyrins, resulting in particles with computed tomography contrast.**

47. Ng KK, Takada M, Jin CCS, Zheng G. Self-sensing porphysomes for fluorescence-guided photothermal therapy. *Bioconjug. Chem.* 26(2), 345–351 (2015).

48. Liu TW, MacDonald TD, Shi J, Wilson BC, Zheng G. Intrinsically copper-64-labeled organic nanoparticles as radiotracers. *Angew. Chem. Int. Ed. Engl.* 51(52), 13128–13131 (2012).

- **Expandes the use of porphysomes to positron emission tomography imaging.**

49. Fathi P, Knox HJ, Sar D *et al.* Biodegradable biliverdin nanoparticles for efficient photoacoustic imaging. *ACS Nano* 13(7), 7690–7704 (2019).

- **The first demonstration of lymph node imaging with biliverdin nanoparticles.**

50. Pan D, Caruthers SD, Hu G *et al.* Ligand-directed nanobialys as theranostic agent for drug delivery and manganese-based magnetic resonance imaging of vascular targets. *J. Am. Chem. Soc.* 130(29), 9186–9187 (2008).

- **One of the earliest demonstrations of MRI with nanoparticles derived from porphyrin-chelated trivalent manganese.**

51. Lee Y, Lee S, Lee DY, Yu B, Miao W, Jon S. Multistimuli-responsive bilirubin nanoparticles for anticancer therapy. *Angew. Chem. Int. Ed. Engl.* 55(36), 10676–10680 (2016).

52. Cui L, Lin Q, Jin CS *et al.* A PEGylation-Free biomimetic porphyrin Nanoplatform for personalized cancer theranostics. *ACS Nano* 9(4), 4484–4495 (2015).

53. Jin CS, Lovell JF, Chen J, Zheng G. Ablation of hypoxic tumors with dose-equivalent photothermal, but not photodynamic, therapy using a nanostructured porphyrin assembly. *ACS Nano* 7(3), 2541–2550 (2013).

54. Fathi P, Capron G, Tripathi I *et al.* Computed tomography-guided additive manufacturing of personalized absorbable gastrointestinal stents for intestinal fistulae and perforations. *Biomaterials* 228, 119542 (2020).

55. Schirra CO, Roessl E, Koehler T *et al.* Statistical reconstruction of material decomposed data in spectral CT. *IEEE Trans. Med. Imaging* 32(7), 1249–1257 (2013).

56. Schirra CO, Senpan A, Roessl E *et al.* Second generation gold nanobeacons for robust K-edge imaging with multi-energy CT. *J. Mater. Chem.* 22(43), 23071–23077 (2012).

57. Pan D, Schirra CO, Senpan A *et al.* An early investigation of ytterbium nanocolloids for selective and quantitative "multicolor" spectral CT imaging. *ACS Nano* 6(4), 3364–3370 (2012).

58. Pan D, Roessl E, Schlomka JP *et al.* Computed tomography in color: nanok-enhanced spectral CT molecular imaging. *Angew. Chem. Int. Ed. Engl.* 49(50), 9635–9639 (2010).

59. Pan D, Williams TA, Senpan A *et al.* Detecting vascular biosignatures with a colloidal, radio-opaque polymeric nanoparticle. *J. Am. Chem. Soc.* 131(42), 15522–15527 (2009).

60. Pan D, Caruthers SD, Senpan A *et al.* Synthesis of NanoQ, a copper-based contrast agent for high-resolution magnetic resonance imaging characterization of human thrombus. *J. Am. Chem. Soc.* 133(24), 9168–9171 (2011).

61. Kim B, Schmieder AH, Stacy AJ, Williams TA, Pan D. Sensitive biological detection with a soluble and stable polymeric paramagnetic nanocluster. *J. Am. Chem. Soc.* 134(25), 10377–10380 (2012).

62. Jin R, Lin B, Li D, Ai H. Superparamagnetic iron oxide nanoparticles for MR imaging and therapy: design considerations and clinical applications. *Curr. Opin. Pharmacol.* 18, 18–27 (2014).

63. Vallabani NVS, Singh S. Recent advances and future prospects of iron oxide nanoparticles in biomedicine and diagnostics. *3 Biotech.* 8(6), 279 (2018).

64. Zanganeh S, Hutter G, Spitler R *et al.* Iron oxide nanoparticles inhibit tumour growth by inducing pro-inflammatory macrophage polarization in tumour tissues. *Nat. Nanotechnol.* 11(11), 986–994 (2016).

65. Thiesen B, Jordan A. Clinical applications of magnetic nanoparticles for hyperthermia. *Int. J. Hyperth.* 24(6), 467–474 (2008).

66. Im J, Lawrence J, Seelig D, Nho RS. FoxM1-dependent RAD51 and BRCA2 signaling protects idiopathic pulmonary fibrosis fibroblasts from radiation-induced cell death article. *Cell Death Dis.* 9(6), 584 (2018).

67. Song KH, Jung SY, Park JI *et al.* Inhibition of karyopherin-α2 augments radiation-induced cell death by perturbing BRCA1-mediated DNA repair. *Int. J. Mol. Sci.* 20(11), 2843 (2019).

68. Bladen CL, Flowers MA, Miyake K *et al.* Quantification of ionizing radiation-induced cell death *in situ* in a vertebrate embryo. *Radiat. Res.* 168(2), 149–157 (2007).

69. Wu L, Cai X, Nelson K *et al.* A green synthesis of carbon nanoparticles from honey and their use in real-time photoacoustic imaging. *Nano Res.* 6(5), 312–325 (2013).

70. Pan D, Cai X, Kim B, Stacy AJ, Wang LV, Lanza GM. Rapid synthesis of near infrared polymeric micelles for real-time sentinel lymph node imaging. *Adv. Healthc. Mater.* 1(5), 582–589 (2012).

71. Pan D, Cai X, Yalaz C *et al.* Photoacoustic sentinel lymph node imaging with self-assembled copper neodecanoate nanoparticles. *ACS Nano* 6(2), 1260–1267 (2012).
72. Pan D, Pramanik M, Senpan A, Wickline SA, Wang LV, Lanza GM. A facile synthesis of novel self-assembled gold nanorods designed for near-infrared imaging. *J. Nanosci. Nanotechnol.* 10(12), 8118–8123 (2010).
73. Pan D, Pramanik M, Senpan A *et al.* Molecular photoacoustic imaging of angiogenesis with integrin-targeted gold nanobeacons. *FASEB J.* 25(3), 875–882 (2011).
74. Pan D, Pramanik M, Senpan A *et al.* Near infrared photoacoustic detection of sentinel lymph nodes with gold nanobeacons. *Biomaterials* 31(14), 4088–4093 (2010).
75. Pan D, Pramanik M, Senpan A *et al.* Molecular photoacoustic tomography with colloidal nanobeacons. *Angew. Chem. Int. Ed. Engl.* 48(23), 4170–4173 (2009).
76. Whittington NC, Wray S. Suppression of red blood cell autofluorescence for immunocytochemistry on fixed embryonic mouse tissue. *Curr. Protoc. Neurosci.* 81, 2.28.1–2.28.12 (2017).
77. Zhao J, Zhong D, Zhou S. NIR-I-to-NIR-II fluorescent nanomaterials for biomedical imaging and cancer therapy. *J. Mater. Chem. B.* 6(3), 349–365 (2018).
78. Li JB, Liu HW, Fu T, Wang R, Zhang XB, Tan W. Recent progress in small-molecule near-IR probes for bioimaging. *Trends Chem.* 1(2), 224–234 (2019).
79. Kim C, Erpelding TN, Jankovic L, Pashley MD, Wang L V. Deeply penetrating *in vivo* photoacoustic imaging using a clinical ultrasound array system. *Biomed. Opt. Express.* 1(1), 278 (2010).
80. Zhang HF, Maslov K, Stoica G, Wang L V. Functional photoacoustic microscopy for high-resolution and noninvasive *in vivo* imaging. *Nat. Biotechnol.* 24(7), 848–851 (2006).
81. Mallidi S, Luke GP, Emelianov S. Photoacoustic imaging in cancer detection, diagnosis and treatment guidance. *Trends Biotechnol.* 29(5), 213–221 (2011).
82. Gutierrez-Juarez G, Gupta SK, Al-Shaer M *et al.* Detection of melanoma cells *in vitro* using an optical detector of photoacoustic waves. *Lasers Surg. Med.* 42(3), 274–281 (2010).
83. Wang X, Xie X, Ku G, Wang LV, Stoica G. Noninvasive imaging of hemoglobin concentration and oxygenation in the rat brain using high-resolution photoacoustic tomography. *J. Biomed. Opt.* 11(2), 024015 (2006).
84. Kruger RA, Kuzmiak CM, Lam RB, Reinecke DR, Del Rio SP, Steed D. Dedicated 3D photoacoustic breast imaging. *Med. Phys.* 40(11), 1–8 (2013).
85. Wang LV, Hu S. Photoacoustic tomography: *in vivo* imaging from organelles to organs. *Science* 335(6075), 1458–1462 (2012).
86. Guggenheim JA, Allen TJ, Plumb A *et al.* Photoacoustic imaging of human lymph nodes with endogenous lipid and hemoglobin contrast. *J. Biomed. Opt.* 20(5), 050504 (2015).
87. Weight RM, Dale PS, Viator JA. Detection of circulating melanoma cells in human blood using photoacoustic flowmetry. *Proceedings of 2009 Annual International Conference of the IEEE Engineering in Medicine and Biology Society.* Minneapolis, MN, USA (3–6 September 2009).
88. Galanzha EI, Shashkov EV, Spring PM, Suen JY, Zharov VP. *In vivo*, noninvasive, label-free detection and eradication of circulating metastatic melanoma cells using two-color photoacoustic flow cytometry with a diode laser. *Cancer Res.* 69(20), 7926–7934 (2009).
89. Longo DL, Stefania R, Aime S, Oraevsky A. Melanin-based contrast agents for biomedical optoacoustic imaging and theranostic applications. *Int. J. Mol. Sci.* 18(8), 1719 (2017).
90. Chitgupi U, Nyayapathi N, Kim J *et al.* Surfactant-stripped micelles for NIR-II photoacoustic imaging through 12 cm of breast tissue and whole human breasts. *Adv. Mater.* 31(40), 1–10 (2019).
91. Liu G, Zhu J, Guo H *et al.* Mo_2C-derived polyoxometalate for NIR-II photoacoustic imaging-guided chemodynamic/photothermal synergistic therapy. *Angew. Chem. Int. Ed. Engl.* 58(51), 18641–18646 (2019).
92. Guo B, Chen J, Chen N *et al.* High-resolution 3D NIR-II photoacoustic imaging of cerebral and tumor vasculatures using conjugated polymer nanoparticles as contrast agent. *Adv. Mater.* 31(25), 1–9 (2019).
93. Jiang Y, Li J, Zhen X, Xie C, Pu K. Dual-peak absorbing semiconducting copolymer nanoparticles for first and second near-infrared window photothermal therapy: a comparative study. *Adv. Mater.* 30(14), 1–7 (2018).
94. Zou L, Wang H, He B *et al.* Current approaches of photothermal therapy in treating cancer metastasis with nanotherapeutics. *Theranostics* 6(6), 762–772 (2016).
95. Riley RS, Day ES. Gold nanoparticle-mediated photothermal therapy: applications and opportunities for multimodal cancer treatment. *Wiley Interdiscip. Rev. Nanomed. Nanobiotechnol.* 9(4), 1446–1452 (2017).
96. Song X, Liang C, Gong H, Chen Q, Wang C, Liu Z. Photosensitizer-conjugated albumin-polypyrrole nanoparticles for imaging-guided *in vivo* photodynamic/photothermal therapy. *Small* 11(32), 3932–3941 (2015).
97. Abrahamse H, Hamblin MR. New photosensitizers for photodynamic therapy. *Biochem. J.* 473(4), 347–364 (2016).

98. Tokura Y, Moriwaki SI. Photodynamic therapy. *Ther. Skin Dis.* 90(12), 105–111 (2010).

99. Espinosa A, Di Corato R, Kolosnjaj-Tabi J, Flaud P, Pellegrino T, Wilhelm C. Duality of iron oxide nanoparticles in cancer therapy: amplification of heating efficiency by magnetic hyperthermia and photothermal bimodal treatment. *ACS Nano* 10(2), 2436–2446 (2016).

100. Li M, Bu W, Ren J *et al.* Enhanced synergism of thermo-chemotherapy for liver cancer with magnetothermally responsive nanocarriers. *Theranostics* 8(3), 693–709 (2018).

101. Lin IC, Fang JH, Lin CT, Sung SY, Su YL, Hu SH. Enhanced targeted delivery of cyclodextrin-based supermolecules by core–shell nanocapsules for magnetothermal chemotherapy. *Macromol. Biosci.* 16(9), 1273–1286 (2016).

102. Yoon HY, Selvan ST, Yang Y *et al.* Engineering nanoparticle strategies for effective cancer immunotherapy. *Biomaterials* 178, 597–607 (2018).

103. Chu D, Zhao Q, Yu J, Zhang F, Zhang H, Wang Z. Nanoparticle targeting of neutrophils for improved cancer immunotherapy. *Adv. Healthc. Mater.* 5(9), 1088–1093 (2016).

104. Mi Y, Smith CC, Yang F *et al.* A dual immunotherapy nanoparticle improves T-cell activation and cancer immunotherapy. *Adv. Mater.* 30(25), 1–9 (2018).

105. Hasegawa Y, Nakamura Y, Choyke PL *et al.* Spatially selective depletion of tumor-associated regulatory T cells with near-infrared photoimmunotherapy. *Sci. Transl. Med.* 8(352), 352ra110–352ra110 (2016).

106. Tanaka T, Osuka A. Conjugated porphyrin arrays: synthesis, properties and applications for functional materials. *Chem. Soc. Rev.* 44(4), 943–969 (2015).

107. Luo L, Liu C, He T *et al.* Engineered fluorescent carbon dots as promising immune adjuvants to efficiently enhance cancer immunotherapy. *Nanoscale* 10(46), 22035–22043 (2018).

108. Seybold PG, Gouterman M. Porphyrins. XIII: fluorescence spectra and quantum yields. *J. Mol. Spectrosc.* 31(1–13), 1–13 (1969).

109. Kongshaug M. Distribution of tetrapyrrole photosensitizers among human plasma proteins. *Int. J. Biochem.* 24(8), 1239–1265 (1992).

110. Zurlo J, Rudacille D, Goldberg AM. *Animals and alternatives in testing: history, science and ethics.* Mary Ann Liebert Inc, NY, USA (1994).

111. Overchuk M, Zheng M, Rajora MA, Charron DM, Chen J, Zheng G. Tailoring porphyrin conjugation for nanoassembly-driven phototheranostic properties. *ACS Nano* 13(4), 4560–4571 (2019).

112. Uttamlal M, Sheila Holmes-Smith A. The excitation wavelength dependent fluorescence of porphyrins. *Chem. Phys. Lett.* 454(4–6), 223–228 (2008).

113. Dayer M, Moosavi-Movahedi A, Dayer M. Band assignment in hemoglobin porphyrin ring spectrum: using four-orbital model of Gouterman. *Protein Pept. Lett.* 17(4), 473–479 (2010).

114. Kou J, Dou D, Yang L. Porphyrin photosensitizers in photodynamic therapy and its applications. *Oncotarget* 8(46), 81591–81603 (2017).

115. Roeder B. Tetrapyrroles: a chemical class of potent photosensitizers for the photodynamic treatment of tumours. *Lasers Med. Sci.* 5(2), 99–106 (1990).

116. Fiel RJ, Musser DA, Mark EH, Mazurchuk R, Alletto JJ. A comparative study of manganese meso-sulfonatophenyl porphyrins: contrast-enhancing agents for tumors. *Magn. Reson. Imaging* 8(3), 255–259 (1990).

117. Place DA, Faustino PJ, Berghmans KK, van Zijl PCM, Chesnick AS, Cohen JS. MRI contrast-dose relationship of manganese(III)tetra(4-sulfonatophenyl) porphyrin with human xenograft tumors in nude mice at 2.0 T. *Magn. Reson. Imaging* 10(6), 919–928 (1992).

118. Fawwaz RA, Winchell HS, Frye F, Hephill W, Lawrence JH. Localization of ^{58}Co and ^{65}Zn-hematoporphyrin complexes in canine lymph nodes. *J. Nucl. Med.* 10(9), 581–585 (1969).

119. Fawwaz RA, Hemphill W, Winchell HS. Potential use of ^{109}Pd-porphyrin complexes for selective lymphatic ablation. *J. Nucl. Med.* 12(5), 231–236 (1972).

120. Takehara Y, Sakahara H, Masunaga H *et al.* Tumour enhancement with newly developed Mn-metalloporphyrin (HOP-9P) in magnetic resonance imaging of mice. *Br. J. Cancer* 84(12), 1681–1685 (2001).

121. Fujimori H, Matsumura A, Yamamoto T *et al.* Tumor specific contrast enhancement study of Mn-metalloporphyrin (ATN-10)–comparison of rat brain tumor model, cytotoxic and vasogenic edema models. *Acta Neurochir.* 70, 167–169 (1997).

122. Schmiedl UP, Nelson JA, Robinsons DH *et al.* Pharmaceutical properties, biodistribution and imaging characteristics of manganese-mesoporphyrin: a potential hepatobiliary contrast agent for magnetic resonance imaging. *Invest. Radiol.* 28(10), 925–932 (1993).

123. Takehara Y, Sakahara H, Masunaga H *et al.* Assessment of a potential tumor-seeking manganese metalloporphyrin contrast agent in a mouse model. *Magn. Reson. Med.* 47(3), 549–553 (2002).

124. Li C, Kräutler B. Transition metal complexes of phyllobilins - a new realm of bioinorganic chemistry. *Dalt. Trans.* 44(22), 10116–10127 (2015).

125. Dimitrijević MS, Bogdanović Pristov J, Žižić M *et al.* Biliverdin-copper complex at physiological pH. *Dalt. Trans.* 48(18), 6061–6070 (2019).

126. Goncharova I, Urbanová M. Vibrational and electronic circular dichroism study of bile pigments: complexes of bilirubin and biliverdin with metals. *Anal. Biochem.* 392(1), 28–36 (2009).

127. Zhou Y, Liang X, Dai Z. Porphyrin-loaded nanoparticles for cancer theranostics. *Nanoscale* 8(25), 12394–12405 (2016).

128. Wang M. Emerging multifunctional NIR photothermal therapy systems based on polypyrrole nanoparticles. *Polymers (Basel)* 8(10), 1–26 (2016).

129. Cai Y, Si W, Huang W, Chen P, Shao J, Dong X. Organic dye based nanoparticles for cancer phototheranostics. *Small* 14(25), 1–17 (2018).

130. Menon RB, Lakshmi VS, Aiswarya MU, Keerthana R, Nair SC. Porphysomes-a paradigm shift in targeted drug delivery. *Int. J. Appl. Pharm.* 10(2), 1–6 (2018).

131. Huynh E, Zheng G. Porphysome nanotechnology: a paradigm shift in lipid-based supramolecular structures. *Nano Today* 9(2), 212–222 (2014).

132. Huynh E, Zheng G. Organic biophotonic nanoparticles: porphysomes and beyond. *IEEE J. Sel. Top. Quantum Electron.* 20(3), 27–34 (2014).

133. Lee Y, Kim H, Kang S, Lee J, Park J, Jon S. Bilirubin nanoparticles as a nanomedicine for anti-inflammation therapy. *Angew. Chem. Int. Ed. Engl.* 55(26), 7460–7463 (2016).

•• **The first demonstration of bilirubin nanoparticle synthesis. Subsequent papers demonstrated a wide variety of applications for these nanoparticles.**

134. Kim JY, Lee DY, Kang S *et al.* Bilirubin nanoparticle preconditioning protects against hepatic ischemia-reperfusion injury. *Biomaterials* 133, 1–10 (2017).

135. Kim MJ, Lee Y, Jon S, Lee DY. PEGylated bilirubin nanoparticle as an anti-oxidative and anti-inflammatory demulcent in pancreatic islet xenotransplantation. *Biomaterials* 133, 242–252 (2017).

136. Kim DE, Lee Y, Kim MG, Lee S, Jon S, Lee SH. Bilirubin nanoparticles ameliorate allergic lung inflammation in a mouse model of asthma. *Biomaterials* 140, 37–44 (2017).

137. Lee DY, Kim JY, Lee Y *et al.* Black pigment gallstone inspired platinum-chelated bilirubin nanoparticles for combined photoacoustic imaging and photothermal therapy of cancers. *Angew. Chem. Int. Ed. Engl.* 56(44), 13684–13688 (2017).

138. Xing R, Zou Q, Yuan C, Zhao L, Chang R, Yan X. Self-assembling endogenous biliverdin as a versatile near-infrared photothermal nanoagent for cancer theranostics. *Adv. Mater.* 31(16), 1–8 (2019).

139. Yang J, Xiong L, Li M *et al.* Preparation and characterization of tadpole- and sphere-shaped hemin nanoparticles for enhanced solubility. *Nanoscale Res. Lett.* 14, 1–9 (2019).

140. Liu Q, Wang H, Shi X, Wang ZG, Ding B. Self-assembled DNA/peptide-based nanoparticle exhibiting synergistic enzymatic activity. *ACS Nano* 11(7), 7251–7258 (2017).

141. Hayashi K, Nakamura M, Miki H *et al.* Near-infrared fluorescent silica/porphyrin hybrid nanorings for *in vivo* cancer imaging. *Adv. Funct. Mater.* 22(17), 3539–3546 (2012).

142. Hayashi K, Nakamura M, Miki H *et al.* Photostable iodinated silica/porphyrin hybrid nanoparticles with heavy-atom effect for wide-field photodynamic/photothermal therapy using single light source. *Adv. Funct. Mater.* 24(4), 503–513 (2014).

143. Ohulchanskyy TY, Roy I, Goswami LN *et al.* Organically modified silica nanoparticles with covalently incorporated photosensitizer for photodynamic therapy of cancer. *Nano Lett.* 7(9), 2835–2842 (2007).

144. Qiu H, Xie J, Che S. Formation of chiral mesostructured porphyrin-silica hybrids. *Chem. Commun.* 47(9), 2607–2609 (2011).

145. Hayashi K, Nakamura M, Ishimura K. Silica-porphyrin hybrid nanotubes for *in vivo* cell tracking by near-infrared fluorescence imaging. *Chem. Commun.* 48(32), 3830–3832 (2012).

146. Lovell JF, Jin CS, Huynh E *et al.* Porphysome nanovesicles generated by porphyrin bilayers for use as multimodal biophotonic contrast agents. *Nat. Mater.* 10(4), 324–332 (2011).

•• **The first reported synthesis of porphysomes, initializing a new category of porphyrin-based nanomaterial.**

147. Liu TW, MacDonald TD, Jin CS *et al.* Inherently multimodal nanoparticle-driven tracking and real-time delineation of orthotopic prostate tumors and micrometastases. *ACS Nano* 7(5), 4221–4232 (2013).

148. MacLaughlin CM, Ding L, Jin C *et al.* Porphyrin lipid nanoparticles for enhanced photothermal therapy in a patient-derived orthotopic pancreas xenograft cancer model. *Mol. Surg. Mol. Devices Appl. II* 9696(8), 96960F (2016).

149. Macdonald TD, Liu TW, Zheng G. An MRI-sensitive, non-photobleachable porphysome photothermal agent. *Angew. Chem. Int. Ed. Engl.* 53(27), 6956–6959 (2014).

150. Muhanna N, Macdonald TD, Chan H *et al.* Multimodal nanoparticle for primary tumor delineation and lymphatic metastasis mapping in a head-and-neck cancer rabbit model. *Adv. Healthc. Mater.* 4(14), 2164–2169 (2015).

151. Jin CS, Overchuk M, Cui L *et al.* Nanoparticle-enabled selective destruction of prostate tumor using MRI-guided focal photothermal therapy. *Prostate* 76(13), 1169–1181 (2016).

152. Ng KK, Takada M, Harmatys K, Chen J, Zheng G. Chlorosome-inspired synthesis of templated metallochlorin-lipid nanoassemblies for biomedical applications. *ACS Nano* 10(4), 4092–4101 (2016).

153. Philp L, Chan H, Rouzbahman M *et al.* Use of porphysomes to detect primary tumour, lymph node metastases, intra-abdominal metastases and as a tool for image-guided lymphadenectomy: proof of concept in endometrial cancer. *Theranostics* 9(9), 2727–2738 (2019).

154. Liu D, Chen B, Mo Y *et al.* Redox-activated porphyrin-based liposome remote-loaded with indoleamine 2,3-dioxygenase (IDO) inhibitor for synergistic photoimmunotherapy through induction of immunogenic cell death and blockage of IDO pathway. *Nano Lett.* 19(10), 6964–6976 (2019).

155. Jin R, Aida T, Inoue S. 'Caged' porphyrin: the first dendritic molecule having a core photochemical functionality. *J. Chem. Soc. Chem. Commun.* 2(1260), 1260–1262 (1993).

156. Cheng L, Wang C, Feng L, Yang K, Liu Z. Functional nanomaterials for phototherapies of cancer. *Chem. Rev.* 114(21), 10869–10939 (2014).

157. Moquin A, Hanna R, Liang T *et al.* PEG-conjugated pyrrole-based polymers: one-pot multicomponent synthesis and self-assembly into soft nanoparticles for drug delivery. *Chem. Commun.* 55(66), 9829–9832 (2019).

158. Alizadeh N, Akbarinejad A. Soluble fluorescent polymeric nanoparticles based on pyrrole derivatives: synthesis, characterization and their structure dependent sensing properties. *J. Mater. Chem. C* 3(38), 9910–9920 (2015).

159. Wu F, Chen L, Yue L *et al.* Small-molecule porphyrin-based organic nanoparticles with remarkable photothermal conversion efficiency for *in vivo* photoacoustic imaging and photothermal therapy. *ACS Appl. Mater. Interfaces* 11, 21408–21416 (2019).

160. Yang L, Li H, Liu D *et al.* Organic small molecular nanoparticles based on self-assembly of amphiphilic fluoroporphyrins for photodynamic and photothermal synergistic cancer therapy. *Colloids Surf. B Biointerfaces* 182, 110345 (2019).

161. Wang D, Niu L, Qiao Z *et al.* Synthesis of self-assembled porphyrin nanoparticle photosensitizers. *ACS Nano* 12(4), 3796–3803 (2018).

162. Wang D, Zhang Z, Lin L *et al.* Porphyrin-based covalent organic framework nanoparticles for photoacoustic imaging-guided photodynamic and photothermal combination cancer therapy. *Biomaterials* 223, 119459 (2019).

163. Pan D, Liang P, Zhong X *et al.* Self-assembled porphyrin-based nanoparticles with enhanced near-infrared absorbance for fluorescence imaging and cancer photodynamic therapy. *ACS Appl. Bio Mater.* 2(3), 999–1005 (2019).

164. Tam NCM, McVeigh PZ, MacDonald TD, Farhadi A, Wilson BC, Zheng G. Porphyrin-lipid stabilized gold nanoparticles for surface enhanced Raman scattering based imaging. *Bioconjug. Chem.* 23(9), 1726–1730 (2012).

165. Ng KK, Lovell JF, Vedadi A, Hajian T, Zheng G. Self-assembled porphyrin nanodiscs with structure-dependent activation for phototherapy and photodiagnostic applications. *ACS Nano* 7(4), 3484–3490 (2013).

166. Trapani M, Castriciano MA, Romeo A *et al.* Nanohybrid assemblies of porphyrin and Au 10 cluster nanoparticles. 9(7), 1026 (2019).

167. Summerfield A, Baldoni M, Kondratuk D V *et al.* Ordering, flexibility and frustration in arrays of porphyrin nanorings. *Nat. Commun.* 10, 2932 (2019).

168. Ghosal K, Ghosh A. Carbon dots: the next generation platform for biomedical applications. *Mater. Sci. Eng. C* 96, 887–903 (2019).

169. Wang J, Qiu J. A review of carbon dots in biological applications. *J. Mater. Sci.* 51(10), 4728–4738 (2016).

170. Liu ML, Chen BB, Li CM, Huang CZ. Carbon dots: synthesis, formation mechanism, fluorescence origin and sensing applications. *Green Chem.* 21(3), 449–471 (2019).

171. Fathi P, Khamo JS, Huang X *et al.* Bulk-state and single-particle imaging are central to understanding carbon dot photo-physics and elucidating the effects of precursor composition and reaction temperature. *Carbon NY* 145, 572–585 (2019).

172. Srivastava I, Khamo JS, Pandit S *et al.* Influence of electron acceptor and electron donor on the photophysical properties of carbon dots: a comparative investigation at the bulk-state and single-particle level. *Adv. Funct. Mater.* 29(37), 1902466 (2019).

173. Ge J, Jia Q, Liu W *et al.* Red-emissive carbon dots for fluorescent, photoacoustic and thermal theranostics in living mice. *Adv. Mater.* 27(28), 4169–4177 (2015).

174. Lee C, Kwon W, Beack S *et al.* Biodegradable nitrogen-doped carbon nanodots for non-invasive photoacoustic imaging and photothermal therapy. *Theranostics* 6(12), 2196–2208 (2016).

175. Lu S, Sui L, Liu J *et al.* Near-infrared photoluminescent polymer–carbon nanodots with two-photon fluorescence. *Adv. Mater.* 29(15), 1–6 (2017).

176. Parvin N, Mandal TK. Dually emissive P,N-co-doped carbon dots for fluorescent and photoacoustic tissue imaging in living mice. *Microchim. Acta* 184(4), 1117–1125 (2017).

177. Bourlinos AB, Bakandritsos A, Kouloumpis A *et al.* Gd(III)-doped carbon dots as a dual fluorescent-MRI probe. *J. Mater. Chem.* 22(44), 23327–23330 (2012).

178. Du F, Zhang M, Ju H *et al.* Engineering iodine-doped carbon dots as dual-modal probes for fluorescence and x-ray CT imaging. *Int. J. Nanomedicine* 10, 6943–6953 (2015).

179. Ren X, Liu L, Li Y, Dai Q, Zhang M, Jing X. Facile preparation of gadolinium(iii) chelates functionalized carbon quantum dot-based contrast agent for magnetic resonance/fluorescence multimodal imaging. *J. Mater. Chem. B* 2(34), 5541–5549 (2014).

180. Su H, Liao Y, Wu F *et al.* Cetuximab-conjugated iodine doped carbon dots as a dual fluorescent/CT probe for targeted imaging of lung cancer cells. *Colloids Surf. B Biointerfaces* 170, 194–200 (2018).

181. Tang J, Kong B, Wu H *et al.* Carbon nanodots featuring efficient FRET for real-time monitoring of drug delivery and two-photon imaging. *Adv. Mater.* 25(45), 6569–6574 (2013).

182. Feng T, Ai X, An G, Yang P, Zhao Y. Charge-convertible carbon dots for imaging-guided drug delivery with enhanced *in vivo* cancer therapeutic efficiency. *ACS Nano* 10(4), 4410–4420 (2016).

183. Gong X, Zhang Q, Gao Y, Shuang S, Choi MMF, Dong C. Phosphorus and nitrogen dual-doped hollow carbon dot as a nanocarrier for doxorubicin delivery and biological imaging. *ACS Appl. Mater. Interfaces* 8(18), 11288–11297 (2016).

184. Liu C, Zhang P, Zhai X *et al.* Nano-carrier for gene delivery and bioimaging based on carbon dots with PEI-passivation enhanced fluorescence. *Biomaterials* 33(13), 3604–3613 (2012).

185. Pierrat P, Wang R, Kereselidze D *et al.* Efficient *in vitro* and *in vivo* pulmonary delivery of nucleic acid by carbon dot-based nanocarriers. *Biomaterials* 51, 290–302 (2015).

186. Wang L, Wang X, Bhirde A *et al.* Carbon-dot-based two-photon visible nanocarriers for safe and highly efficient delivery of siRNA and DNA. *Adv. Healthc. Mater.* 3(8), 1203–1209 (2014).

187. Lan M, Zhao S, Zhang Z *et al.* Two-photon-excited near-infrared emissive carbon dots as multifunctional agents for fluorescence imaging and photothermal therapy. *Nano Res.* 10(9), 3113–3123 (2017).

188. Zheng M, Li Y, Liu S, Wang W, Xie Z, Jing X. One-pot to synthesize multifunctional carbon dots for near infrared fluorescence imaging and photothermal cancer therapy. *ACS Appl. Mater. Interfaces* 8(36), 23533–23541 (2016).

189. Ge J, Jia Q, Liu W *et al.* Carbon dots with intrinsic theranostic properties for bioimaging, red-light-triggered photodynamic/photothermal simultaneous therapy *in vitro* and *in vivo*. *Adv. Healthc. Mater.* 5(6), 665–675 (2016).

190. Wen Y, Jia Q, Nan F *et al.* Pheophytin derived near-infrared-light responsive carbon dot assembly as a new phototheranotic agent for bioimaging and photodynamic therapy. *Chem. Asian J.* 14(12), 2162–2168 (2019).

191. Wu F, Su H, Wang K, Wong WK, Zhu X. Facile synthesis of N-rich carbon quantum dots from porphyrins as efficient probes for bioimaging and biosensing in living cells. *Int. J. Nanomedicine* 12, 7375–7391 (2017).

192. Li Y, Zheng X, Zhang X *et al.* Porphyrin-based carbon dots for photodynamic therapy of hepatoma. *Adv. Healthc. Mater.* 6(1), 1–6 (2017).

•• **One of the earliest reports of carbon dots formed from porphyrins.**

193. Wu F, Su H, Cai Y, Wong WK, Jiang W, Zhu X. Porphyrin-implanted carbon nanodots for photoacoustic imaging and *in vivo* breast cancer ablation. *ACS Appl. Bio Mater.* 1(1), 110–117 (2018).

194. Zhao J, Huang M, Zhang L *et al.* Unique approach to develop carbon dot-based nanohybrid near-infrared ratiometric fluorescent sensor for the detection of mercury ions. *Anal. Chem.* 89(15), 8044–8049 (2017).

195. Li XG, Li A, Huang MR, Liao Y, Lu YG. Efficient and scalable synthesis of pure polypyrrole nanoparticles applicable for advanced nanocomposites and carbon nanoparticles. *J. Phys. Chem. C.* 114(45), 19244–19255 (2010).

196. Wang X, Qu K, Xu B, Ren J, Qu X. Multicolor luminescent carbon nanoparticles: synthesis, supramolecular assembly with porphyrin, intrinsic peroxidase-like catalytic activity and applications. *Nano Res.* 4(9), 908–920 (2011).

197. Arcudi F, Dordevic L, Prato M. Synthesis, separation and characterization of small and highly fluorescent nitrogen-doped carbon nanodots. *Angew. Chem. Int. Ed. Engl.* 55(6), 2107–2112 (2016).

198. Huang P, Lin J, Wang X *et al.* Light-triggered theranostics based on photosensitizer-conjugated carbon dots for simultaneous enhanced-fluorescence imaging and photodynamic therapy. *Adv. Mater.* 24(37), 5104–5110 (2012).

199. Shan L, Fan W, Wang W *et al.* Organosilica-based hollow mesoporous bilirubin nanoparticles for antioxidation-activated self-protection and tumor-specific deoxygenation-driven synergistic therapy. *ACS Nano* 13(8), 8903–8916 (2019).

200. Yang X, Lu Y. Preparation of polypyrrole-coated silver nanoparticles by one-step UV-induced polymerization. *Mater. Lett.* 59(19–20), 2484–2487 (2005).

201. Takahashi Y, Furukawa Y, Ishida T, Yamada S. Site-selective nanoscale-polymerization of pyrrole on gold nanoparticles via plasmon induced charge separation. *Nanoscale* 8(16), 8520–8524 (2016).

202. Zotti G, Vercelli B, Berlin A. Gold nanoparticles linked by pyrrole- and thiophene-based thiols. Electrochemical, optical and conductive properties. *Chem. Mater.* 20(2), 397–412 (2008).

203. Ujiie H, Ding L, Fan R *et al.* Porphyrin–high-density lipoprotein: a novel photosensitizing nanoparticle for lung cancer therapy. *Ann. Thorac. Surg.* 107(2), 369–377 (2019).

204. Kamkaew A, Lim SH, Lee HB, Kiew LV, Chung LY, Burgess K. BODIPY dyes in photodynamic therapy. *Chem. Soc. Rev.* 42(1), 77–88 (2013).

205. Wu F, Chen L, Yue L *et al.* Small-molecule porphyrin-based organic nanoparticles with remarkable photothermal conversion efficiency for *in vivo* photoacoustic imaging and photothermal therapy. *ACS Appl. Mater. Interfaces.* 11(24), 21408–21416 (2019).